Oct10, 2017

Dear editor,

The manuscript: ***Black carbon and mineral dust in snow cover on the Tibetan Plateau*** by Zhang Y.L. et al.

The manuscript number: tc-2017-111

We greatly appreciate the reviewers' constructive comments to improve the paper. We have revised our manuscript according to these comments (blue color in the main text), and hope the revised manuscript is suitable for publication in The Cryosphere.

The "point to point" response to comments are listed as below.

Sincerely yours,
Yulan Zhang and Shichang Kang

Response to Referee #2

This manuscript presents results from snow sampling, laboratory analysis, and related modeling efforts for the presence and impact of light absorbing impurities in the Tibetan Plateau region. Although the manuscript is not wrong in stating more measurements are valuable in constraining our understanding of the spatial and temporal variability of light absorbing particulates, the techniques presented in this paper are unclear and as written does not contribute to the state of knowledge of light absorbing particulates in snow. Major changes are needed before this paper can be reviewed again for publication. I will not, at the point, do line by line corrections because they are numerous. The authors need to revisit the writing in each section for editing and to clarify there justification, methods, and results. Particularly, snow sampling and automatic weather stations need to be described in significantly more detail.

Answer: Thank you very much for the comments and suggestions. We have tried to improve the methods and results in the main text (in blue color). Snow sampling and automatic weather stations are also described in detailed (Section2.2, Section3.3, in blue color).

Comment 1: My first and foremost concern is that samples were collected in November and December, and yet they are attempting to quantify the impacts of light absorbing particulates on melt. This does not make sense to me and if I misunderstood this it is because it is not made clear in the manuscript. Although the sample collection timing may be after the summer monsoon, these samples do not represent the impurities that are present during the ablation season- and therefore it is inappropriate to use these values to quantify reduction in snowpack duration. Particularly for dust, which tends to deposit in the spring when source regions dry out (peak radiative forcing by dust in snow is observed from MODIS imagery over the Himalayan region in April and May).

Answer: Agree, these samples were collected during winter season when the snow cover were more stable and continuous, which might not represent the true impurities as these during the ablation season. However, during melting season, because of the poor accessibility on the snowpack in the TP, it was hardly to collect the snow cover samples. Besides, considerable heterogeneity in the topography and climate has led to complex spatial and temporal snow cover patterns (Xu et al., 2017). Discontinued snow cover during melting season may be a problem to represent the true impurities in snow. Thus in our study, we gave an estimation based on the different snow grain size and density, rather than the fixed data. We have to admit there existed uncertainties at present. In the future, we should do more related works to fill in gaps.

Comment 2: The backtrajectory footprint modeling was also very unclear to me, how the model runs were carried out needs to be described better, but it is unclear to me why the model runs were only completed for the winter. And were they run continuously? Typically particulates are deposited in episodic events so running it continuously does not inform the source region, it just informs of the regional synoptics. I suggest seeing Skiles et al., 2015 (Hydrological Processes) for how that study produced and described backtrajectory footprints.

Answer: We agree. Since most of the snow cover will not exist during summer season in the TP, thus we only calculated the model runs in winter when the snow cover accumulated. The calculation is continuous in the winter season since we did not know the exact snow events during the periods. It is an estimation of all air mass which can be transported to the sampling sites.

We have learned the recommended reference (Skiles et al., 2015), and tried to improve the descriptions in the main text as following (Page6, Line6-34).

Calculation of air parcel trajectories is a widely used approach in different areas of atmospheric research. Conceptually, footprint analysis was considered as changes in concentration at the receptor site that can be attributed to different upwind source areas along the backward trajectories (Skiles et al., 2015). To determine the potential origins of the LAIs deposited on the snow cover of the TP, back trajectory analyses were performed using the European Centre for Medium-Range Weather Forecasts (ECMWF) analysis fields with the Lagrangian analysis tool LAGRANTO (Sprenger and Wernli, 2015), launched every six hours for six selected sampling sites as receptors (including three sites of MYL, NMC, and SETP in region I, two sites of TGL and NETP in region II, and LHG in region III) during the winter season. The ECMWF fields (horizontal and vertical wind components) were retrieved on 137 model levels and then interpolated onto a 0.25º×0.25º latitude-longitude grid. Trajectory starting positions can be defined easily and flexibly based on different geometrical and meteorological conditions; after the computation of the trajectories, a versatile selection is offered based on single or combined criteria (Sprenger and Wernli, 2015). First, starting positions are initialized with a suitable domain over the TP at 12:00 UTC on November 1, 2015 (or 2014). For this case, a domain from 0 to 75 and 60 °E to 120 °E was chosen. We choose starting positions in this domain that are horizontally equidistant with 80 km horizontal spacing and extend vertically from 1030 to 790 hPa with 30 hPa vertical spacing. Then, the trajectories are calculated from all starting positions 96 h backward in time. Finally, biomass burning emission data is traced along the calculated trajectories to estimate whether an air parcel at the receptor site is influenced by BC fire emissions or not. In this study, the Fire INventory from NCAR (FINN) v1.5 global fire emissions flux in 2012−2014, speciated with the GEOS-chem mechanism, was used to estimate contributions

of BC fire emission at the six selected receptor sites. FINN emission estimates are based on the framework described by Wiedinmyer et al. (2011). FINN used the satellite observations of active fires and land cover, together with emission factors and estimated fuel loadings to provide daily, highly resolved (1 km) open biomass burning emissions estimates for use in regional and global chemical transport models. Then, the same calculation was performed for the Eclipse V5 inventory for the anthropogenic contributions of BC. The Eclipse V5 inventory was widely used in the simulations. The historical data for the period 1990−2010 were revised compared to preceding sets using the latest IAE (the International Energy Agency) and FAO (the Food and Agriculture Organization) statistics extending to 2010, as well as recent country reporting where available. Note that this analysis was not exactly quantitative and did not take into account wet and dry deposition. We also assumed that the anthropogenic emissions have not changed significantly from 2010 compared to the period from 2012−2014. Thus, the comparison of natural and anthropogenic BC contributions was reasonable. The relative differences between the BC contributions can provide information on regional differences in this study.

References:

Skiles, S. M., Painter, T. H., belnap, J., Holland, L., Reynolds, R. L., Goldstein, H. L., Lin, J.: Regional variability in dust-on-snow processes and impacts in the Upper Colorado River Basin, Hydrol. Process., doi:10.1002/hyp.10569, 2015.

Comment 3: The albedo measurements need to be better described. And how was snow effective grain radius retrieved? This should be an optically equivalent grain size, not an observable grain size. If an effective/optical grain size was used, the retrieval should be described. If observed grain sizes were used, the large error introduced by this (see Painter et al., 2007 in Journal of Glaciology) needs to be mentioned. Estimates of changes in snow cover duration should be removed or significant more detail and justification needs to be made for the timing of sample collection.

Answer: In this study, we used an optically equivalent grain size, not an observable grain size.

In the field, the snow grains were sprayed on the MIG paper. Then we took a photo by using portable digital microscope (Anyty 3R-MSV500) (Fig. R1a). In the lab, we can measure the snow grain shape and obtain the lengths of a and b (Fig. R1b). Mugnai and Wiscombe (1987) demonstrated that a collection of unoriented non-spheroids produce the same scattering results as spheres, and Grenfell and Warren (1999) showed that the radius of a non-spherical particle was equal to that of a spherical particle that has the same volume-to-surface-area (V/A) ratio. Consequently, V/A ratio was used to transfer the measured snow grain size into the effective grain size.

On this basis of field measurement, Hao (2009) proposed two assumptions: 1) The snow particle is an inequilateral spheroid; and 2) The major axis, minor axis, and height of the inequilateral spheroid is denoted by a, b, and c, respectively, in such a way that the relationship a = 2b exists. According to Kokhanovsky and Zege (2004), the effective snow grain radius (R_{ef}) can be calculated equal to the radius of the volume-to-surface equivalent sphere by the following equation (1):

$$R_{ef} = \frac{3\bar{V}}{4\bar{A}} \quad (1)$$

Where, $\bar{V} = \frac{4}{3}\pi r^3$ and $\bar{A} = \pi r^2$, are the average volume and the average cross-section (geometric

shadow) area of the snow grains, respectively. And, *r* is the radius of geometric optics, $r = \frac{a+b}{4}$.

Thus, $R_{ef} \approx 0.35a$

Eq.1 was then employed to calculate the effective snow grain size.

We have added related information in the main text (Page 5, Line2-12):

For the snow grain size observation, we sprayed the snow grains on MIG paper and took a photo using a portable digital microscope (Anyty 3R-MSV500) to calculate the major and minor axis (Fig. S2). Based on field measurements from previous studies (Mugnai and Wiscombe, 1980; Grenfell and Warren, 1999), two assumptions were proposed: 1) The snow grain particle is an inequilateral spheroid, and 2) The major axis (a), minor axis (b), and height (c) of the inequilateral spheroid are denoted by a, b, and c, respectively, in such a way that the relationship a=2b exists (Hao, 2009). According to Kokhanovsky and Zege (2004), the effective snow grain radius (R_{ef}) can be calculated as equal to the radius of the volume-to-surface equivalent sphere by the following equation (1):

$$R_{ef} = \frac{3\bar{V}}{4\bar{A}} \quad (1)$$

where $\bar{V} = \frac{4}{3}\pi r^3$ and $\bar{A} = \pi r^2$, are the average volume and the average cross-section (geometric shadow) area of the snow grains, respectively. In addition, *r* is the radius of geometric optics, $r = \frac{a+b}{4}$.

Thus

$$R_{ef} \approx 0.35a \quad (2)$$

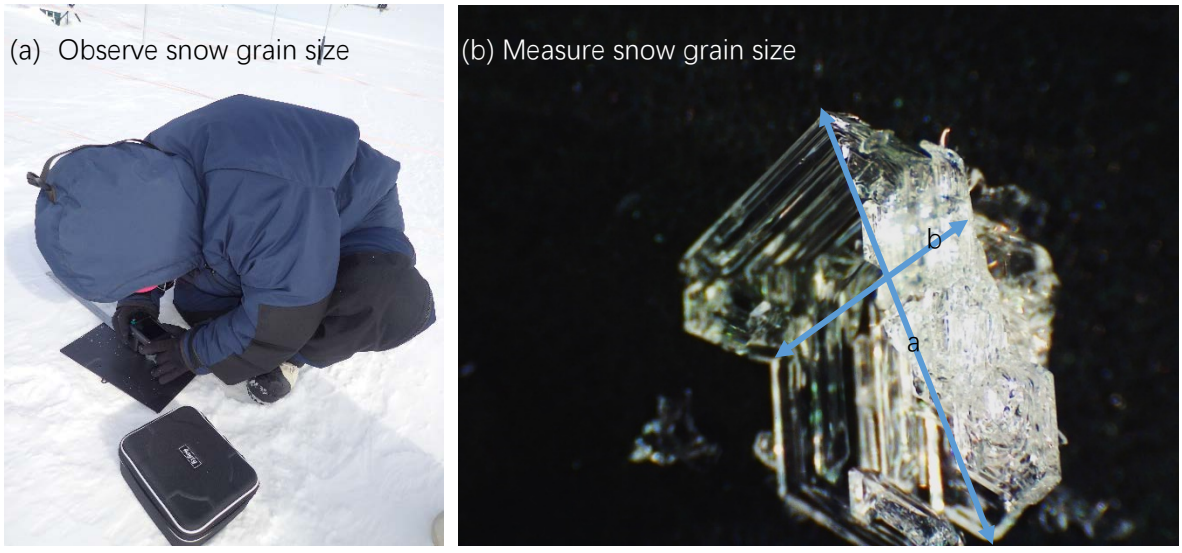

Figure R1. Snow grain size observation in the field (a) and measurement in the lab (b).

For the estimates of changes in snow cover duration days, we have tried to improve the related details in the main text.

References:

Grenfell, T. C., and Warren, S. G.: Representation of a nonspherical ice particle by a collection of independent sphere for scattering and obsorption of radiation, J. geophys. Res., 104(D24), 31697–31709, 1999.

Hao, X.: Retrieval of alpine snow cover area and grain size basing on optical remote sensing. PhD thesis, Cold and Arid Regions Environment Engineering Research Institute, Lanzhou, China, pp. 103–104, 2009.

Mugnai, A., and Wiscombe, W. J.: Scattering of radiation by moderately nonspherical particles. J. Atmos. Sci., 37, 1291–1307, 1987.

Comment 4: Section 3.3 and 3.4 are generally confusing- was shortwave radiation (uplooking and downlooking pyranometers) actually measured? This analysis seems far too simplified. Furthermore, the discussion of snow depth is misleading. This is a straightforward energy balance calculation, so less snow will melt faster than more snow for an equal amount of forcing- this is basic mass balance. So snow depth does not itself play an important role in the reduction of snow cover by particulates. This is a mixing up of forcing and state functions. The citations are also outdated or incorrect in many cases, and I suggest the authors revisit these.

Answer: Shortwave radiation data used in this study was actually measurement by automatic weather station at different selected site near the snow sampling sites in region I, II, and III of the TP (Fig R2). Table R1 showed monthly short-wave radiation from automatic weather stations near the snow sampling sites during the snow melting season (March-May) when the temperature began to increase. On average, shortwave radiations in March, April, May, and June is about 238, 269, 292, and 271 W m^{-2}, respectively. Short-wave radiation in March showed the minimum value in Tanggula (210 W m^{-2}, lower than the average). Short-wave radiation in May showed the maximum value in Namco (314 W m^{-2}, higher the average). Thus, in order to estimate the impact of input short-wave radiation on the snow cover duration, we gave a range of short-wave radiation from 220 to 310 W m^{-2}.

We have added related information in the main text as following (Page11, Line14-23):

In Eq. (4), monthly shortwave radiation (*SW*) input data were obtained from the Automatic Weather Station (AWS) near the snow sampling sites across the TP (Fig. S3). Table S3 shows monthly shortwave radiation data from AWS during the snow melting season (March-May) when the temperature began to increase. On average, shortwave radiation in March, April, May, and June is approximately 238, 269, 292, and 271 W m^{-2}, respectively. Short-wave radiation in March showed the minimum value in Tanggula of the central TP (210 W m^{-2}, lower than the average), whereas in May it showed the maximum value in Namco (314 W m^{-2}, higher the average). Based on these data during the melt season, three scenarios (220, 270, and 310 W m^{-2})were defined as the minimum, median, and maximum scenarios of input shortwave radiation to estimate its impact on changes of snow cover duration.

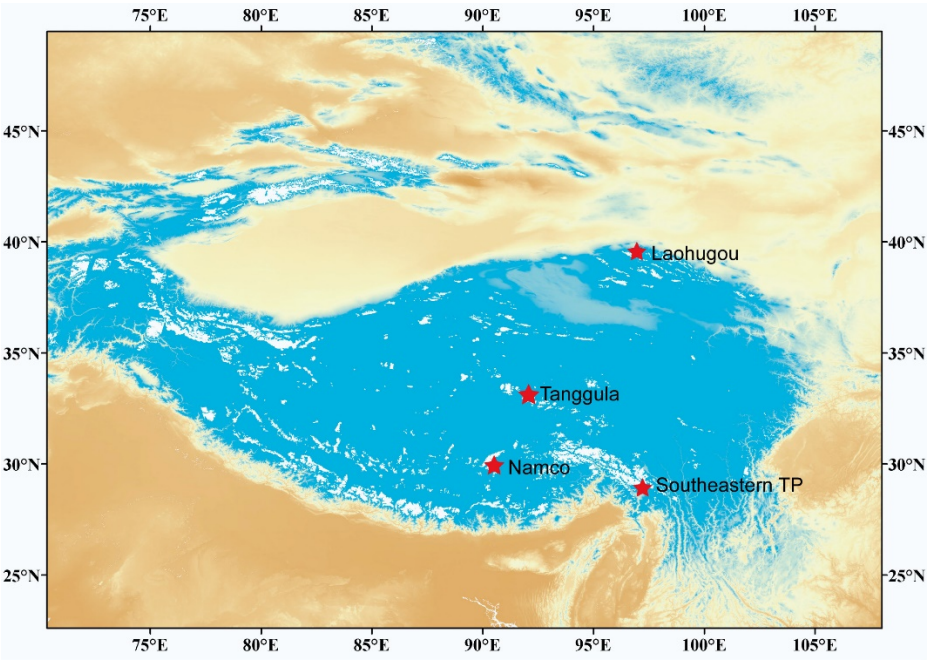

Figure R4. Automatic weather stations selected in the Tibetan Plateau.

Table R1. Monthly short-wave radiation from automatic weather stations near the snow sampling sites during the snow melting season.

Sites	Month of the year	Monthly Short-wave radiation (W m^{-2})	Month of the year	Monthly Shortwave radiation (W m^{-2})
Southeastern Tibetan Plateau				
	March in 2014	**248**	March in 2015	**237**
	April in 2014	**288**	April in 2015	**259**
	May in 2014	**305**	May in 2015	**280**
	June in 2014	**265**	June in 2015	**250**
Namco				
			March in 2015	**264**
			April in 2015	**276**
			May in 2015	**306**
			June in 2015	**314**
Tanggula				
	March in 2014	**210**		
	April in2014	**226**		
	May in 2014	**245**		
	June in 2014	**271**		
Laohugou				
	March in 2014	**229**	March in 2015	**238**
	April in2014	**269**	April in 2015	**294**
	May in 2014	**311**	May in 2015	**305**
	June in 2014	**258**	June in 2015	**269**

We agree that the equation for changes of snow cover duration is a straightforward energy balance calculation. Thus in this study, it means the duration days of less snow will be less than the more snow for an equal amount of forcing. So under the same level of LAIs in snow, the reduction of snow cover duration days can be affected by different snow depth. We have tried to revise in the main text (section 3.4).

Comment 5: I take issue with the use of the 'Third Pole' term, this is not universally recognized and is somewhat politicized, why not just use Tibetan Plateau or High Mountain Asia? Also light absorbing impurity is an outdated term, the community has moved toward the use of light absorbing particulates. Also mineral dust and the acronym MD are confusing you can simply say dust- which needs no acronym. Similarly, please be consistent in terminology, for example, albedo and reflectance are not the same thing.
Answer: We have changed the term "Third Pole" to be "Tibetan Plateau".

We have used the term "light-absorbing particulates" in the main text.

We have changed the "MD" as "dust" in the main text.

Albedo and reflectance are not the same thing. Albedo is defined as the ratio of irradiance reflected to the irradiance received by a surface. The proportion reflected is not only determined by properties of the surface itself, but also by the spectral and angular distribution of solar radiation reaching the Earth's surface. Unless given for a specific wavelength (spectral albedo), albedo refers to the broadband spectrum of solar radiation.

Reflectance of the surface of a material is its effectiveness in reflecting radiant energy. It is the fraction of incident electromagnetic power that is reflected at an interface. The reflectance spectrum or spectral reflectance curve is the plot of the reflectance as a function of wavelength. When we use ASD, we get the reflectance. In order to compare the albedo simulated by SNICAR model in this study, we have to calculate the reflectance based on the standard solar irradiance.
We also carefully use the words consistent in the main text.

Comment 6: Uncertainties in modeling are not only due to lack of observations, and increasing our number of sampling points alone will not reduce our model uncertainty. To state this is misleading.
Answer: Agree, and we have tried to revise this section in the section3.4 of the main text.

Black carbon and mineral dust in snow cover on the Tibetan Plateau

Yulan Zhang[1], Shichang Kang[1,2*], Michael Sprenger[3], Zhiyuan Cong[2], Tanguang Gao[4], Chaoliu Li[2], Shu Tao[5], Xiaofei Li[1], Xinyue Zhong[1], Min Xu[1], Wenjun Meng[5], Xiang Qin[1], Mika Sillanpää[6]

[1]State key laboratory of Cryospheric Science, Northwest Institute of Eco-Environment and Resources, Chinese Academy of Sciences, Lanzhou730000, China
[2]CAS Center for Excellence in Tibetan Plateau Earth Sciences, Beijing 100101, China
[3]Institute for Atmospheric and Climate Science, ETH Zurich, CH-8092 Zurich, Switzerland
[4]Key Laboratory of Western China's Environmental System (Ministry of Education), College of Earth and Environmental Sciences, Lanzhou University, Lanzhou 730000, China
[5]Department of Environmental Science, Laboratory for Earth Surface Processes, Peking University, Beijing, China
[6]Laboratory of Green Chemistry, Lappeenranta University of Technology, Mikkeli 50130, Finland

Correspondence to: Prof. Shichang Kang (shichang.kang@lzb.ac.cn)

Abstract. Snow cover plays a key role for sustaining ecology and society in mountainous regions. Light-absorbing particulates (including black carbon, organic carbon, and mineral dust) deposited on snow can reduce surface albedo and contribute to the near-worldwide melting of snow cover and ice. This study focused on understanding the role of black carbon and other water-insoluble light-absorbing particulates in the snow cover of the Tibetan Plateau (TP). The results found that the black carbon, organic carbon, and dust concentrations in snow cover generally ranged from 202–17 468 ng g^{-1}, 491–13 880 ng g^{-1}, and 22–846 μg g^{-1}, respectively, with higher concentrations in the central to northern areas of the TP. Footprint analyses suggested that the northern TP was influenced mainly by air masses from Central Asia with some Euro-Asia influence, and air masses in the central and Himalayan region originated mainly from Central and South Asia. The biomass burning sourced black carbon contributions decreased from ~50 % in the southern TP to ~30 % in the northern TP. The contribution of black carbon and dust to snow albedo reduction reached approximately 37 % and 15 %, respectively. The effect of black carbon and dust reduced the average changes of snow cover duration by 3.1±0.1 days to 4.4±0.2 days. Meanwhile, the black carbon and dust had important implications for snowmelt water loss over the TP. The findings indicate that the impacts of black carbon and mineral dust need to be properly accounted for in future regional climate projections, particularly in the high-altitude cryosphere.

1 Introduction

Black carbon (BC), organic carbon (OC), and mineral dust (hereafter: dust) are the main constituents of light-absorbing particulates (LAPs) in snow (Andreae and Gelencsér, 2006; Bond et al., 2013; Di Mauro et al., 2015; Doherty et al., 2010; Painter et al., 2010). LAPs can reduce snow and ice albedo and trigger positive feedbacks that contribute to the near-worldwide melting of snow cover and ice (Dumont et al., 2014; Flanner et al., 2007; Hadley and Kirchstetter, 2012; Hansen and Nazarenko, 2004; Painter et al., 2013; Zhang et al., 2017). Atmospheric BC is a distinct type of carbonaceous material from incomplete

combustion of biomass/biofuel and fossil fuel. A large fraction of BC is emitted from anthropogenic activities (Bond et al., 2013). Because BC can absorb solar radiation, influence cloud processes, and alter the melting of snow cover and glaciers, it has been considered to be the second most important climate forcer in the Earth's climate system only after carbon dioxide (Andreae and Ramanathan, 2013; Bond et al., 2013; Ramanathan and Carmichael, 2008). Model studies in recent decades indicated that BC in seasonal snow may be responsible for a significant impact on warming and albedo reduction over the Arctic (Flanner, 2013; Qian et al., 2014), Greenland (Dumont et al., 2014), the Alps (Painter et al., 2013; Yasunari et al., 2015), and the Tibetan Plateau (TP) (He et al., 2014; Jacobi et al., 2015; Ji et al., 2015; Ménégoz et al., 2014). The snow albedo feedback of BC may also be an important driver accelerating glacial retreat and snow cover melt (Painter et al., 2013; Skiles et al., 2015; Xu et al., 2009).

Light-absorbing OC in snow can contribute significantly to the absorption by ultraviolet/visible light (Andreae and Gelencsér, 2006; Yan et al., 2016). Bahadur et al. (2012) studied aerosol optical properties derived from the Aerosol Robotic Network (AERONET) measurements and estimated that, in California, the OC absorption at 440 nm was approximately 40 % of the BC absorption. Measurements of hundreds of snow samples revealed that approximately 40 % of the light absorption from impurities in Arctic snow and sea ice is due to non-BC constituents (Doherty et al., 2010). In western North America, Dang and Hegg (2014) suggested that OC was responsible for more than 10 % of the total light absorption. A global model by Lin et al. (2014) estimated the role of OC in the reduction of snow albedo and the simulation showed that the radiative forcing (RF) of OC deposited in land snow and sea ice ranges from +0.0011 to +0.0031 W m^{-2} or as large as 24 % of the forcing caused by BC in snow and ice. The RF of snow pit dissolved organic carbon (DOC) from a Tibetan glacier was calculated to be 0.43 W m^{-2}, indicating that DOC in snow needs to be taken into consideration in accelerating glacial melt on the TP (Yan et al., 2016).

Mineral dust, another important LAP component in snow cover, can change the cryospheric environment and hydrological cycle due to its light-absorbing properties (Di Mauro et al., 2015; Ji et al., 2016a; Painter et al., 2010, 2013; Wu et al., 2016; Zhang et al., 2015). In the European Alps, observed reflectance provided evidence that seasonal input of dust can strongly decrease the spectral properties of snow, in particular, from 350 to 600 nm (Di Mauro et al., 2015, 2017). In a study of two sites on Claridenfirn of the Swiss Alps, Gabbi et al. (2015) showed that mineral dust lowered the mean annual albedo by 0.006–0.011, depending on the location on the glacier, causing a reduction of approximately 142–271 mm in annual mass balance. In the San Juan Mountains of the USA, snow cover duration in a seasonal snow-covered region, was found to be shortened by 18 to 35 days during ablation through surface shortwave RF caused by deposition of disturbed desert dust (Painter et al., 2007). In the upper Colorado River Basin, the daily spring dust RF ranged from 30−65 W m^{-2}, advancing melt by 15-49 days (Skiles et al., 2015). A study of the Mera glacier on the southern slope of the Himalayas even indicated that, when dust concentrations are high, dust dominates absorption, snow albedo reduction, and RF, and the impact of BC may be negligible (Kaspari et al., 2014). The presence of dust in snow suggests a relevant role for BC in darkening the glacier surface.

As an important component of the hydrology, snow cover plays a key role for sustaining ecology and society in mountainous regions (Beniston et al., 2017). Snowpack changes are not only crucial for estimating impacts on water resources but also important to anticipate natural hazards related to snow avalanches/disasters (Beniston et al., 2017; Brown and Mote, 2009).

Covered by a large volume of snow/ice in the mid-low latitudes, the TP is considered to be a sensitive and readily visible indicator of climate change (Yao et al., 2012a). Recently, the TP cryosphere has undergone rapid changes (Kang et al., 2010), including glacial shrinkage (Xu et al., 2009; Yao et al., 2012b), permafrost degradation (Cheng and Wu, 2007), and reduction in the annual duration of snow cover days (Ménégoz et al., 2014; Xu et al., 2017). Studies on the TP indicate that BC has been a significant contributing factor to the observed cryospheric change (Li et al., 2017; Ming et al., 2009; Niu et al., 2017; Xu et al., 2009;Yang et al., 2015; Zhang et al., 2017), and a major forcer of climate change (Qian et al., 2015; Ji, 2016a). Observations and simulations also found that dust deposition on snow/ice can change the surface albedo and perturb the surface radiation balance (Ji et al., 2016b; Qu et al., 2014), causing a decrease of 5–25 mm snow water equivalent (mm w.e.) over the western TP and Himalayas (Ji et al., 2016b).

Changes in snow cover over the TP have attracted much attention in recent years owing to climate change (Xiao and Duan, 2016; Xu et al., 2017). Snow cover on the TP plays an important role in the Asian summer monsoon, and serves as a crucial water source for several major Asian rivers (Bai and Feng, 1994; Lau et al., 2010; Vernekar et al., 1995; Yao et al., 2012a; Zhao and Moore, 2004). Atmospheric heating related to BC and dust deposition can lead to widespread enhanced warming over the TP and accelerated snowmelt in the western TP and Himalayas (Lau et al., 2010; Ramanathan and Carmichael, 2008; Zhang et al., 2015). Simulation studies of BC in snow over the TP have inherent uncertainties due to the physics/chemistry/transport scheme used in the models (Gertler et al., 2016; Yasunari et al., 2010, 2013). For example, Kopacz et al. (2011) estimated RF of 5 to 15 W m^{-2} due to BC within the snow-covered areas of Himalaya and the TP, whereas Flanner et al. (2007) and Qian et al. (2011) estimated peak values of BC effects exceeding 20 W m^{-2} for some parts of the TP. Menon et al. (2010) and Ménégoz et al. (2014) proposed that during the last decade BC in snow caused a significant part of the decrease of the snow cover extent or duration observed on the TP during the last decade. Ji et al. (2016b) found a positive surface RF was induced by dust, which caused a decrease of 5–25 mm w.e. over the western TP, Himalayas, and Pamir Mountains from December to May. Large-area observations of BC data in snow cover, which are still seldom in the TP, can be useful for model evaluation and calibration in the future.

To further understand the role of BC and dust in TP snow cover, more measurements and an extended LAP dataset of snow cover properties is needed to study their effects on cryospheric change in future of this region. This study is an attempt to fill this gap. Snow cover samples were collected across the TP in winter seasons (Fig. 1, Table S1), which will provide the first large-area survey of BC and dust in seasonal snow cover over the TP, investigate albedo reduction and RF, and estimate changes of snow cover duration days caused by LAPs. Footprint analysis coupled with BC fire emission inventory will approximately constrain BC natural/anthropogenic contributions. The results of this study will increase understanding of BC and dust in snow cover across the TP and enable improved climate modeling, and this is also helpful for mitigation actions around the Tibetan cryospheric region.

2 Methodology

2.1 Study area

The TP covers an area of more than 2.5 million km^2 with an average elevation greater than 4000 m a.s.l. (Yao et al., 2012a). The TP exerts profound influences on atmospheric circulation and climate through mechanical and thermal effects because of its large area, unique topography, and geographical location in the earth system (Yanai and Wu, 2006). Extended glacial coverage (over 100,000 km^2) and snow cover have the potential to modify regional hydrology and trigger natural hazards that can impact local populations, agriculture, and water resources in and around the region (e.g., Immerzeel et al., 2010; Xu et al., 2009; Yao et al., 2012a).

Moderate Resolution Imaging Spectroradiometer (MODIS) data from 2000–2006 showed that the spatial distribution of snow cover is quite variable over the TP because of the complex terrain (Pu et al., 2007). Maximum snow accumulation and melting times vary over the year but are generally later as the elevation increases. Additionally, large interannual variabilities occur in the late autumn and winter months. Heating by light-absorbing aerosols produces an atmospheric dynamic feedback, which increases moisture, cloud cover, and deep convection over northern India, and enhances the rate of snow melt in the Himalayas and the TP (Lau et al., 2010; Ramanathan and Carmichael, 2008). The accelerated melting of snow is confined mostly to the western TP, beginning slowly in early April and then progressing more rapidly from early to mid-May; the snow cover remains reduced from mid-May through early June (Lau et al., 2010). The decadal change in the spring snow depth over the TP can impact on the Asian summer monsoon and a close relationship exists between the interdecadal increase of snow depth over the TP during March–April, increased summer rainfall over the Yangtze River valley, and a dryer summer along the southeast coast of China and the Indochina peninsula (Zhang et al., 2004). Based on observations from 103 meteorological stations across the TP, the duration of snow cover exhibited a significant decreasing trend (1.2 days per decade), which was jointly controlled by a later snow starting time (1.6±0.8 days per decade) and an earlier snow ending time (−1.9±0.8 days per decade) consistent with a response to climate change (Xu et al., 2017).

2.2 Sample collection

For this study, snow cover samples were collected at 37 sites (Fig. 1a) and one glacial river basin (Laohugou region, including 10 sites as in Fig. 1b) across the TP in December 2014 and November 2015 (Table S1). As shown in Figure 1a, these field campaigns can be grouped into three regions, as was done in previous studies (Yao et al., 2013). Region I (Southern TP) includes 27 sites and is mainly affected by the Indian monsoon. Region II (Central TP) contains 10 sites that are affected by both the westerlies and the Indian monsoon. Intensified sampling (10 sites) has been carried out in the LHG region within Region III, which is located in the northeastern part of the TP. Seasonal snow samples (34) were also collected from the 10 sites in the LHG region of Qilian Mountain (Fig. 1b) from December 2015 to June 2016.

To minimize the effects of local sources, we selected sampling sites more than 1 km away from roads and usually 30 km from villages and cities. Generally, snow samples were collected from the top 5−10 cm with cleaned stainless-steel utensils, and

placed in Whirl-Pak® bags (Fig. S1). These snow samples were kept frozen until they underwent filtration. During sampling, snow depth, grain size, and density were also observed. For the snow grain size observation, we sprayed the snow grains on MIG paper and took a photo using a portable digital microscope (Anyty 3R-MSV500) to calculate the major and minor axis (Fig. S2). Based on field measurements from previous studies (Mugnai and Wiscombe, 1980; Grenfell and Warren, 1999), two assumptions were proposed: 1) The snow grain particle is an inequilateral spheroid, and 2) The major axis (a), minor axis (b), and height (c) of the inequilateral spheroid are denoted by a, b, and c, respectively, in such a way that the relationship a=2b exists (Hao, 2009). According to Kokhanovsky and Zege (2004), the effective snow grain radius (R_{ef}) can be calculated as equal to the radius of the volume-to-surface equivalent sphere by the following equation (1):

$$R_{ef} = \frac{3\bar{V}}{4\bar{A}} \quad (1)$$

where $\bar{V} = \frac{4}{3}\pi r^3$ and $\bar{A} = \pi r^2$, are the average volume and the average cross-section (geometric shadow) area of the snow grains, respectively. In addition, r is the radius of geometric optics, $r = \frac{a+b}{4}$.

Thus, $R_{ef} \approx 0.35a$ (2)

2.3 LAP measurements

In the laboratory, the snow samples were melted rapidly in a hot-water bath to minimize the melt time. Immediately after melting, the snow samples were filtered through pre-baked quartz filters (Whatman™) using an electric pump to create a partial vacuum. Then, sample meltwater was saved in polyethylene bottles, and refrozen for chemical analysis.

Because the mineral dust mass is much larger than the BC and OC mass in the snow samples compared to aerosol samples (Wang et al., 2012), dust concentrations were calculated by taking the difference in the weight of the quartz filter before and after filtration. Quartz filters were then used to analyze BC and OC with a thermal-optical carbon analyzer (DRI 2001A model, Desert Research Insitute, NV, USA) following a methodology (IMPROVE_A protocol) used in previous studies (Cao et al., 2003; Chow et al., 2004; Xu et al., 2009; Yang et al., 2015). Its function relies on the fact that OC components can be volatilized from the sample and deposited in a non-oxidizing helium atmosphere, in which BC can be combusted with an oxidizer. The sample punch is placed in a quartz holder oriented in the direction of the carrier gas flow, and heated gradually to a special temperature (typically 550 or 850 ℃) in a pure helium atmosphere, which results in volatilization of the OC in the sample. Then, the temperature rises and the punch is reheated stepwise to near 900 ℃ in an oxygen-containing atmosphere (usually 2 % oxygen and 98 % helium) to burn out all carbon remaining (BC). The carbon released from each temperature plateau is converted to methane and measured by a flame ionization detector. Due to the influence of dust on the quantitative analysis of BC and OC in snow when using a thermal optical method (Wang et al., 2012), we modified the method so that in a 100 % helium atmosphere, only a temperature plateau (550 ℃) was arranged to reduce the time that BC was exposed to a catalyzing atmosphere (Yang et al., 2015). Under ideal conditions, the minimum detection limit of total carbon is 0.93 μg C cm^{-2}, with a range of 0.2−750 μg C cm^{-2}. During the experiments, the filter blank (detected by blank filters) was 1.23 ±0.38 μg C cm^{-2}.

To identify uncertainty stemming from instrumental instability and the uneven distribution of carbon particles in the filters, duplicates of ~30 % of the samples were analyzed separately, with consistent results (BC r^2=0.95, OC r^2=0.87, dust r^2=0.90). Because we analyzed the filters through which the melted snow samples passed, the OC measured in our study was water-insoluble OC.

2.4 Footprint analysis

Calculation of air parcel trajectories is a widely used approach in different areas of atmospheric research. Conceptually, footprint analysis was considered as changes in concentration at the receptor site that can be attributed to different upwind source areas along the backward trajectories (Skiles et al., 2015). To determine the potential origins of the LAPs deposited on the snow cover of the TP, back trajectory analyses were performed using the European Centre for Medium-Range Weather Forecasts (ECMWF) analysis fields with the Lagrangian analysis tool LAGRANTO (Sprenger and Wernli, 2015), launched every six hours for six selected sampling sites as receptors (including three sites of MYL, NMC, and SETP in region I, two sites of TGL and NETP in region II, and LHG in region III) during the winter season. The ECMWF fields (horizontal and vertical wind components) were retrieved on 137 model levels and then interpolated onto a 0.25 °×0.25 °latitude-longitude grid. Trajectory starting positions can be defined easily and flexibly based on different geometrical and meteorological conditions; after the computation of the trajectories, a versatile selection is offered based on single or combined criteria (Sprenger and Wernli, 2015). First, starting positions are initialized with a suitable domain over the TP at 12:00 UTC on November 1, 2015 (or 2014). For this case, a domain from 0 to 75 and 60 °E to 120 °E was chosen. We choose starting positions in this domain that are horizontally equidistant with 80 km horizontal spacing and extend vertically from 1030 to 790 hPa with 30 hPa vertical spacing. Then, the trajectories are calculated from all starting positions 96 h backward in time. Finally, biomass burning emission data is traced along the calculated trajectories to estimate whether an air parcel at the receptor site is influenced by BC fire emissions or not. In this study, the Fire INventory from NCAR (FINN) v1.5 global fire emissions flux in 2012−2014, speciated with the GEOS-chem mechanism, was used to estimate contributions of BC fire emission at the six selected receptor sites. FINN emission estimates are based on the framework described by Wiedinmyer et al. (2011). FINN used the satellite observations of active fires and land cover, together with emission factors and estimated fuel loadings to provide daily, highly resolved (1 km) open biomass burning emissions estimates for use in regional and global chemical transport models. Then, the same calculation was performed for the Eclipse V5 inventory for the anthropogenic contributions of BC. The Eclipse V5 inventory was widely used in the simulations. The historical data for the period 1990−2010 were revised compared to preceding sets using the latest IAE (the International Energy Agency) and FAO (the Food and Agriculture Organization) statistics extending to 2010, as well as recent country reporting where available. Note that this analysis was not exactly quantitative and did not take into account wet and dry deposition. We also assumed that the anthropogenic emissions have not changed significantly from 2010 compared to the period from 2012−2014. Thus, the comparison of natural and anthropogenic BC contributions was reasonable. The relative differences between the BC contributions can provide information on regional differences in this study.

2.5 Reflectance measurements and albedo simulations

For the selected sites, a general-purpose spectroradiometer (Analytical Spectral Devices (ASD), FieldSpec 4, Inc.), was used to measure the reflectance of snow cover. The ASD FieldSpec 4 instrument is a general-purpose spectroradiometer that is useful for applications requiring the measurement of reflectance, transmittance, radiance, or irradiance. The instrument is specifically designed for field environment remote sensing to acquire visible and near-infrared and shortwave infrared spectra. It has 3 nm spectral resolution on the visible/near infrared detector (350–1050 nm, silicon photodiode array), and 10–12 nm resolution on the shortwave infrared detectors (900–2 500 nm, InGaAs). In the field, reflectance was measured at two sites (24K and MD in Table S1) with FieldSpec 4 under clear-sky conditions. These measurements of reflectance were calculated using the standard solar irradiance to get the albedos, which were then used for comparison with simulated albedos.

Albedo reduction caused by LAPs is calculated by the SNow ICe and Aerosol Radiation (SNICAR) model (Flanner et al., 2007), which utilizes the two-stream radiative transfer solution of Toon et al. (1989) and has been widely used in Arctic snow (e.g., Flanner et al., 2007, 2009; Hadley and Kirchstetter, 2012). This simulator provides hemispheric reflectance of snow for unique combinations of impurity content (black carbon, dust, and volcanic ash), snow grain size, and incident solar flux characteristics. The input fields include incident radiation, solar zenith angle, surface spectral distribution, effective snow grain radius, snow cover thickness and density, albedo of the underlying ground, and concentrations of impurities. Based on our observations, the effective snow grain radius ranged from approximately 100 to 1500 μm for different snow samples based on calculation of Eq. (2), and snow density ranged from 150 to 400 kg m^{-3}. These two factors varied in low, medium, and high scenarios in the model runs (Table 1).

In terms of the albedo calculation, RF due to BC and dust can be obtained by using Eq. (3) (Kaspari et al., 2014; Yang et al., 2015):

$$\mathrm{RF} = \sum_{0.325\ \mu m}^{2.505\ \mu m} E(\lambda, \theta)\,(\alpha_{(r,\lambda)} - \alpha_{(r,\lambda,imp)})\Delta\lambda \quad (3)$$

where α is the modeled snow spectral albedo with or without the impurities (imp) of BC and/or dust; E is the spectral irradiance; r is the snow optical grain size; λ is wavelength (μm); and θ is the solar zenith angle for irradiance.

In general, the snow cover is vertically inhomogeneous, and sometimes it is optically thin (Voisin et al., 2012). The stratified structure of snow cover will lead to the discrepancy between computed spectral albedo from semi-infinite snow cover and measured albedo (Grenfell, 1994; Aoki et al., 2000; Zhou et al., 2003; Kuipers Munneke et al., 2008). In this study, we usually collected snow samples from the top 5−10 cm. Because the SNICAR model is a single-layer implementation model (Flanner et al., 2007, 2009), the input parameter of "snowpack thickness" was the observed snow cover depth.

2.6 Estimates of changes in snow cover duration

To estimate snow melt due to BC and dust, a method was constructed in which the absorptivity of the snow was multiplied by the daily average incoming shortwave radiation from the automatic weather stations (AWS) set up at the meteorological stations near the sampling sites (Fig. S3) (Schmale et al., 2017). Factors derived from meteorological stations in the adjacent

areas included daily temperature and daily solar shortwave insolation. Average albedo reductions for snow cover by BC and dust were derived from the SNICAR model. To calculate the amount of snow melted based on the enthalpy of fusion of water (334 J g^{-1}), the snow cover was assumed to be at 0 ℃ and then snowmelt was calculated by using Eq. (4) (Schmale et al., 2017):

$$\mathrm{Melt}_{snow} = \mathrm{N}_{Tht0} \times \Delta\alpha \times SW \quad (4)$$

where N_{Tht0} is the number of days with temperature greater than 0 ℃; Δα is the albedo reduction caused by BC and dust, for clean snow mainly by different snow grain sizes due to snow aging; and *SW* is the shortwave radiation. From Eq. (4), we can estimate changes of snow cover duration (ΔD) based on the observed snow depth. We expressed the results for each case as low, medium, and high scenarios, based on albedo variations.

3 Results and discussion

3.1 Distributions of LAPs

Across the TP, most of the samples we took were old wind-packed snow. Generally, the ground layer of snow was usually depth hoar, similar to that in Arctic snow (Doherty et al., 2010) and central North American snow (Doherty et al., 2014, 2016). For many of these sampling sites, the snow cover was intermittent (Fig. S1). During the winter season, surface soil can be carried aloft by strong winds and deposited on snow cover, which affects the concentrations of LAPs (Wang et al., 2013). Our results indicated that the spatial distributions of BC, OC, and dust in snow over the TP generally ranged from 202–17,468 ng g^{-1}, 491–13,880 ng g^{-1}, and 22–846 μg g^{-1}, respectively (Fig. 2). Variations in the concentrations of LAPs were higher in the central to northern TP (Region II and III) than in the southern TP (Region I) (Table 2). The highest concentrations may be related to the lower snow depth and dirtier snow that resulted from post-deposition processes (e.g., snow at some sites was melting). In Region I, the snow was cleaner and had lower concentrations of LAPs comparable to concentrations in the old snow of glaciers (Kaspari et al., 2014).

The previous studies also examined concentrations of LAPs in snow from central North America (Doherty et al., 2014, 2016; Skiles and Painter, 2016; Zatko et al., 2016), northern China (Huang et al., 2011; Wang et al., 2013; Ye et al., 2012), Japan (Kuchiki et al., 2015), Europe (Chýlek et al., 1987), the Arctic (Doherty et al., 2010; Forsström et al., 2013), Greenland (Aoki et al., 2014; Zatko et al., 2013), and Antarctic (Warren and Clark, 1990; Zatko et al., 2013). Concentrations of BC and other water-insoluble LAPs from the TP were most similar to those in the snow from northern China (Wang et al., 2013), but higher than those from the Himalayas (Lim et al., 2014) (Table 2). In comparison (Table 2), the LAPs in snow cover of the TP showed larger values which can be attributed to more deposition from nearby regions around the TP (e.g., South Asia, East Asia, and/or western China) (Lu et al., 2012; Ramanathan and Carmichael, 2008), or to impacts by the soil near the sampling sites.

Ratios of OC to BC (OC/BC) were used to represent the possible impact of biomass burning in previous studies (Watson et al., 2001; Bond et al., 2013; Cong et al., 2015a, 2016b). Usually, the aerosols emitted from biomass burning have higher OC/EC ratios. For example, Watson et al. (2001) reported an OC/EC ratio of 14.5 for forest fires; whereas for fossil fuel, the

OC/EC ratio was approximately 1. The OC/BC ratio in our sampled surface snow ranged from 0.64 to 3.31 over the TP, generally decreasing from south to north (Fig. 2d). The average ratios for Regions I, II, and III were 1.82, 1.31, and 1.14, respectively (Table 2), indicating a decreasing impact of biomass-sourced aerosol deposition in snow over the TP. The little higher OC/BC in region I may be due to its proximity to South Asian combustion sources dominated by biomass burning (Cong et al., 2015a, 2015b; Li et al., 2016). For example, in the LHG region, lower LAP concentrations in fresh clean snow were observed at LHG3 and LHG6 (Fig. 1b), whereas near the glacier at LHG1 and LHG2, the collected wind packed, aged snow samples were quite dirty, and had higher LAP concentrations (Fig. 3a, b, and c). Meanwhile, OC/BC ratios were lower at sites near the glacier (Fig. 3d), implying predominantly non-biomass sourced combustion. Higher ratios of OC/BC were found at the sites near human settlements (LHG7–10) (Fig. 3d), where there was extensive biofuel combustion (e.g., yak dung or straw burning). Because of the variations in sampling periods, snow types and depths, sources of dust and carbonaceous aerosol deposition, and/or strong winds, these results were expected to vary with large uncertainties. In general, however, anthropogenic activities play an important role in the ratios of OC/BC in snow cover.

Figure 4 shows the footprint analyses arrived at for selected sites across the TP in winter. The northern TP sites (LHG and NETP) are influenced mainly by air masses from Central Asia and partly by air masses from Euro-Asia, which are similar to the sources of dust reaching the TP (e.g., Zhang et al., 2016). These results are also consistent with those of He et al. (2014), Kopacz et al. (2011), and Lu et al. (2012), who modeled contributions of BC emissions in the same region. In the central (TGL and NMC) and southern region (MYL and SETP) of the TP, the air masses originate mainly from Central and South Asia. Anthropogenic BC emissions dominate the BC snow albedo as shown in previous studies (Li et al., 2016; Lu et al., 2012). Contributions of BC from open fire burning (a kind of biomass burning) decrease from the southern to the northern TP (Fig. 5). In the Himalayan region, BC from biomass burning sources accounts for half of the BC deposition on snow cover, reflecting the proximity to large sources in South Asia. In the central TP, BC from open fire burning accounts for approximately 30 % of the total, less than from biomass burning evidence from aerosols and glacial snow (Li et al., 2016), maybe indicating a lack of biofuel contributions from our calculation. Whereas in the northern TP, anthropogenic BC emissions (more than 70 %) dominate the BC albedo reduction. Li et al. (2016), using the $\Delta^{14}C/\delta^{13}C$ compositions of BC isolated from aerosols and snowpit samples in the TP, also found equal contributions from biomass and fossil fuel combustion in the Himalayan region (near the southern TP), whereas BC in the remote northern TP is predominantly derived from fossil fuel combustion (66±16 %). These differences can also be seen from the BC emissions that arrived at the selected sites based on BC inventory data for the year of 2013 (PKU-BC-2013, Wang et al., 2014) in Figure S3. In the southern TP (MYL), the amount of BC deposition is larger than in the northern TP (NETP) due to the nearby BC sources in south Asia, known to be a regional hotspot of BC-induced atmospheric solar heating (Ramanathan and Carmichael, 2008). Whereas in the central TP (NMC), the amount of BC deposition was higher than in the NETP. This may be because pollutants from the southern side of the Himalayas can traverse the high mountain range not only through the major north-south river valleys but also by being lifted and advected over the Himalayas to reach to the inland TP (Cong et al., 2015b; Lüthi et al., 2015).

3.2 Impacts of LAPs on albedo reduction and radiative forcing

To simulate albedo change and surface RF from BC and dust in snow cover, the multi-layer SNICAR model was used (Flanner et al., 2007). Effective snow grain size and snow density was considered at the low, medium, and high scenarios (Table 1) and the SNICAR model was run for clear-sky conditions on the specific sampling days (Table S2).

The SNICAR model simulated albedo (caused by BC and dust with snow grain effective radius=150 μm) matches observed reflectance in both the visible and absorptive near-infrared (Fig. 6). The BC strongly reduces visible reflectance (in particular, from 350–800 nm) but has negligible influence at wavelengths beyond 1 μm, since the impact of snow grain size is large in this wavelength range (Flanner et al., 2007; Gardner and Sharp, 2010). The presence of dust also decreases the albedo in the visible wavelength, which is in agreement with a study of the impact of dust on snow radiative properties conducted in the European Alps (Di Mauro et al., 2015). The difference between measured and simulated reflectance by dust may be caused by the upper boundary of particle size in the SNICAR model (Flanner et al., 2007). The broadband albedo is comparable to albedo simulated for the wavelengths from 350–2500 nm, with albedo differences less than 0.0058 (~2.3 %) (Table 3). For the same wavelengths (350–2500 nm), albedo between measurements and simulations differs less than 0.0155 (~4 %) (Table 3).

For different scenarios defined by the effective snow grain size and snow density in Table 1, clean snow albedos resulting from snow aging range from 0.5992 to 0.7751 (Table 4). If BC or dust is the only impurity in the snow cover, contributions to albedo reduction can reach approximately 37 % or 15 %, respectively, with associated larger RF due to BC. On average, BC and dust contribute to albedo reduction at approximately 0.18 ± 0.01 and 0.06 ± 0.004, respectively (Fig. 7). The total albedo reduction contributed by BC and dust is approximately 38 %, with the associated RF of 18–32 W m^{-2} (Fig. 7). This highlights the importance of LAPs in snow when testing regional- to global-scale models.

Large uncertainties exist in the estimation of BC snow albedo forcing over the TP. Simulation results using the Community Atmosphere Model version 3.1 showed that the aerosol-induced snow albedo perturbations generate surface radiative flux changes of 5–25 W m^{-2} in spring (Qian et al., 2011). Using the SNICAR model coupled a general circulation model, Flanner et al. (2007) showed that, during some spring months, snow-only forcing exceeded 10 and 20 W m^{-2} over parts of the TP. RF in the snow-covered regions due to BC by the GEOS-Chem model induced the snow-albedo effect to vary from 5–15 W m^{-2} over the TP, an order of magnitude larger than RF as a result of the direct effect (Kopacz et al., 2011). Recently, simulation results using a global chemical transport model in conjunction with a stochastic snow model and a radiative transfer model showed an annual mean BC snow albedo forcing to be 2.9 W m^{-2} averaged over snow-covered plateau regions, which is a factor of three larger than the value over global land snow cover (He et al., 2014). Surface RF (simulated by a regional climate model coupled with an aerosol–snow/ice feedback module) induced by dust-in-snow showed positive values in the range of 0–6 W m^{-2} over the interior of the TP, the Himalayas, Pamir, and Tienshan Mountains (Ji et al., 2016b). BC-in-snow/ice can cause positive surface RF (3.0–4.5 W m^{-2}) over the western TP in the monsoon season, with the maximum RF (5–6 W m^{-2}) simulated in the Himalayas and southeastern TP in the non-monsoon season (Ji et al., 2016a). Limited

measurements of LAPs in snow cover over the TP have hindered a more robust estimate of the forcing by BC and dust-in snow in this region (Bond et al., 2013; Qian et al., 2015). The mean forcing of BC and dust in snow in our study is slightly higher than previous results from snowpits (e.g., Ming et al., 2009) and comparable to some parts of the TP in spring (20 W^{-2}) (Flanner et al., 2007), which indicates that more frequent impurity measurements in terms of different years and locations over the TP are necessary for model validation.

Light-absorbing OC in atmospheric aerosols has various origins, e.g., soil humics, humic-like substances (HULIS), tarry materials from combustion, bioaerosols, etc. (Andreae and Gelensc ér, 2006). The chemical and optical properties of OC may differ due to the nature of the OC source or atmospheric processing (Chen and Bond, 2010). In contrast, and in comparison to black carbon and mineral dust, the optical properties of OC in snow/ice have hardly been examined. Due to the lack of reliable OC optical properties that span the dimensions of snow grain size and OC particle size, the SNICAR model currently does not support the calculation of OC-in-snow forcing in the same way as BC. Thus, in this study, we didn't state the effect of OC on albedo reduction and RF.

3.3 Changes in snow cover duration days

Changes of snow cover duration are calculated using a model documented by Schmale et al. (2017) (section 2.6). In Eq. (4), monthly shortwave radiation (*SW*) input data were obtained from the Automatic Weather Station (AWS) near the snow sampling sites across the TP (Fig. S3). Table S3 shows monthly shortwave radiation data from AWS during the snow melting season (March-May) when the temperature began to increase. On average, shortwave radiation in March, April, May, and June is approximately 238, 269, 292, and 271 W m^{-2}, respectively. Short-wave radiation in March showed the minimum value in Tanggula of the central TP (210 W m^{-2}, lower than the average), whereas in May it showed the maximum value in Namco (314 W m^{-2}, higher the average). Based on these data during the melt season, three scenarios (220, 270, and 310 W m^{-2})were defined as the minimum, median, and maximum scenarios of input shortwave radiation to estimate its impact on changes of snow cover duration. The average Snow depth water equivalent (SD, mm) was assumed from previous studies in this region (Che et al., 2012; Xu et al., 2017; Zhong et al., 2016). In general, the number of reduction days in snow cover duration is larger for low scenarios than for medium and high scenarios (Fig. 8 and Table 5), particularly when *SW* input data is lower (220 W m^{-2}). If SD was 40 mm, the average snow cover duration days would be reduced by 1.26 ±0.05 days (*SW*=310 W m^{-2}) to 1.77 ±0.07 days (SW=220 W m^{-2}) by BC and dust (Fig. 8a, c, and e). If SD was 100 mm, the average snow cover duration days would be shortened by 3.14 ±0.13 days to 4.43 ±0.18 days from the effect of BC and dust, with a maximum of approximately 9.4 days (Fig. 8b, d, and f), indicating advanced melt during ablation season. The result indicated that estimation of changes of snow cover duration days caused by the same level of LAPs was also affected by different SD. For different scenarios, dust contributes only approximately 1 day to the reduction of snow cover duration days (Fig. 8 and Table 5). These results imply that the reduction in snow cover duration related to LAPs is due mainly to BC. Note that no significant differences in reductions of snow cover duration are found across the TP (Fig. S4).

Against the background of climate change, changes in duration of snow cover have important consequences for surface energy and water budgets over a range of scales, as well as for cryospheric ecosystems (e.g., Euskirchen et al., 2007; Yuan et al., 2016; Zeeman et al., 2017). Based on measurements and modeling, several studies have documented recent trends toward accelerated snowmelt and changes in snow cover duration caused by BC and dust across the Himalayan-TP in response to enhanced albedo reduction (Ménégoz et al., 2014; Menon et al., 2010; Xu et al., 2009). Ji et al. (2016a, 2016b) noted that BC and dust in snow/ice decreases surface albedo and causes the snow water equivalent to decrease by 5–25 mm over the TP. Ménégoz et al. (2014) has estimated that both dry and wet BC depositions affect the snow cover, reducing its annual duration by 1 to 8 days, which may potentially influence sustaining seasonal water availability (Immerzeel et al., 2010; Tahir et al., 2015).

3.4 Limitations and implications for snow cover and glaciers on the TP

We calculated the effect of LAPs on snow cover duration with a range of simplistic assumptions based on simulations of albedo reduction and RF. We did not consider meteorological conditions, including clouds, precipitation, etc. Snow metamorphism was also not considered, and in the simulation, snow grains were assumed to be spherical, as previous studies (Flanner et al., 2007; Ginot et al., 2013; Schmale et al., 2017). We also did not consider the BC morphology and its mixing state, and light-absorbing properties of OC and dust, which may also significantly affect the light absorption in the simulation (Andreae and Gelencsér, 2006; Kaspari et al., 2014; Di Mauro et al., 2015; Painter et al., 2010; Schmale et al., 2017). BC in the atmosphere tended to mix with OC and inorganic salts during aging enhancing its absorption (Gustafsson and Ramanathan, 2016). He et al. (2014) noted that BC-snow internal mixing increases the albedo forcing by 40–60 % compared with external mixing, and coated BC increases the forcing by 30–50 % compared with uncoated BC aggregates, whereas Koch snowflakes reduce the forcing by 20–40 % relative to spherical snow grains. A lack of OC simulaton due to the limitation of the SNICAR model also affected the results in this study. Due to its light-absorbing properties (Andreae and Gelencsér, 2006; Bahaur et al., 2012; Yan et al., 2016), OC in snow cover can also absorb solar radiation and reduce the surface albedo. Previous studies indicated that OC was responsible for more than 10–40 % of the light absorption (Dang and Hegg, 2014; Doherty et al., 2010; Lin et al., 2014; Wang et al., 2015). Not considering OC in snow will underestimate the LAP impact on albedo reduction and RF, and this should not be ignored in the future.

We also have to pay attention to the fact that dust optical properties depend strongly on source material and their properties are designed to represent "global-mean" characteristics as closely as possible (Flanner et al., 2007). The light absorption by mineral dust in snow is thought to be due to iron oxides (Wang et al., 2013), which are efficient light scattering and absorption materials that can enhance absorption at UV and visible wavelengths (Di Mauro et al., 2015; Moosmüller et al., 2012; Zhang et al., 2015). Goethite and hematite are the most abundant forms of iron oxide in dust and the major light absorbers in the shortwave spectrum in snow (Wu et al., 2016). The SNICAR model applies the Maxwell-Garnett approximation for combining indices of refractions, assuming a mixture of quartz, limestone, montmorillonite, illite, and hematite. We should note that some dust particles (e.g., those containing a large proportion of strongly absorbing hematite) can have a larger impact on snow albedo than the dust applied in this work (Aoki et al., 2006; Painter et al., 2007).

It is further important to note that a large fraction of such uncertainty can also result from uncertainty in the simulated snow-cover fraction/snow depth across the plateau. The TP covers a large area (more than 2.5 million km^2) with an average elevation exceeding 4000 m a.s.l. (Yao et al., 2012a). Considerable heterogeneity in the topography and climate has led to complex spatial and temporal snow cover patterns (Xu et al., 2017). Most studies on the snow cover distribution were based on satellite-based observations (Che et al., 2008, 2012). Surface observations of snow depth showed an increase over the TP from 1957–1998 (Ma and Qin, 2012). However, snow cover depth and the number of snow covered days during the current decade under intense climate warming showed a negative trend mainly occurring in the southeast TP in winter. Whereas in spring, snow cover depth showed a positive trend in the eastern TP (Xu et al., 2017). These differences can also affect the estimation in this study. Nevertheless, the method provides a theoretical approach for evaluating how the presence of LAPs affects the lower parts of the glacier subjected to summer melt.

Snow cover durations were shortened during the melt season as estimated in this study, and the glaciers over western China have been undergoing extensive recession, with an estimated loss of about ~450 km^3 w.e. in volume and 10 % reduction in area during the last 40 years (Yao et al., 2012b). Recently, the annual mass budget of glaciers over the TP was estimated at approximately 15–20 Gt yr^{-1} based on GRACE and ICESat (Gardner et al., 2013; Neckel et al., 2014). These melt waters may affect water resources and social development in the surrounding areas, e.g., India and China (Immerzeel et al., 2010). The total amount of snowmelt caused by LAPs can be estimated over the whole TP using the model described in Sec. 2.6. The number of days with average temperature above 0 ℃ was assumed to be 70 (±25 %) based on the observations from AWS during the melting season. Thus, based on the daily snowmelt (0.76±0.40, 0.67±0.36, and 0.54±0.28 cm w.e. d^{-1} for *SW* at 220, 270, and 310 W m^{-2}, respectively) caused by BC and dust in this study, the estimation shows that approximately 4.61±2.49 Gt yr^{-1} (range of 3.80±1.97 to 5.36±2.78 Gt yr^{-1}) of snowmelt water has been lost due to the effect of BC and dust in snow (Fig. 9). This indicates that glacial snowmelt caused by LAPs contributes ~20 % of total mass balance and that BC and dust may play an important role in recent accelerated snow and glacial melt. However, this result has large uncertainties associated with the lack of sufficient *in situ* and distributed observations of spectral albedo, concentrations of LAPs, and coincident changes in glacier mass observations, as discussed by many previous studies (e.g., Ginot et al., 2014; Ménégoz et al., 2014; Qian et al., 2015; Schmale et al., 2017).

Our study confirms that BC and dust in snow and ice can darken the surface, and further reduce snow albedo, and increase the speed of snow cover melt (e.g., Flanner et al., 2007; Di Mauro et al., 2015; Painter et al., 2007; Qian et al., 2015; Skiles et al., 2015). Thus, the impacts of BC and other LAPs need to be properly accounted for in future regional climate projections, particularly in the high-altitude cryosphere. It is also important to note that, without large scale, *in situ* observation data applied to calibrate BC forcing and constrain simulated values, the impact of BC and other LAPs on the albedo feedback would have been marginal. Schmale et al. (2017) noted that, due to the decreasing trend of dust emissions in Central Asia (Xi and Sokolik, 2015), dust may become less important, while BC deposition may increase as a result of projected increased emissions (Wang et al., 2014). Constraints on BC sources/deposition and climatic/hydrological effects will provide guidance for effective mitigation actions.

4 Conclusions

This study was a large area survey of snow cover over the TP across regions with different climatology and sources of LAPs. Systematically higher values of snow BC concentrations were observed in the central to northern TP (Regions II and III) than in the southern TP (Region I). This finding may be related to shallower snow depths and dirtier snow in Regions II and III as a result of post-depositional processes (e.g., snowdrift, or melting). In the southern TP (Region I), the collected snow was cleaner with lower concentrations of LAPs comparable to concentrations in the glacial aged snow. The ratios of OC/BC in the surface snow samples ranged from 0.64 to 3.31 across the TP, generally decreasing from south to north, which may indicate that anthropogenic activities played an important role on OC/BC ratios in snow cover in the TP region. Footprint analysis also indicated that anthropogenic sourced BC accounted for approximately 70 % of total BC deposition in the central and northern TP. Estimates of albedo reduction contributed by BC and dust were approximately 38 %, with an associated RF of 18–32 W m^{-2}.

The reported shortage of snow cover duration days across the TP relied on single site observations rather than a large area survey. For different scenarios with different SD and shortwave radiation input data, the advanced melt days of snow cover duration related to LAPs was mainly due to BC, which reduced from several days to more than one week. Dust contributed only approximately 1 day to the reduction of snow cover duration days. No significant differences among reductions in snow cover duration were found across the whole TP. The changing snow cover duration may potentially influence seasonal water availability and sustainability.

Furthermore, the estimated effects of BC and dust on glaciers and snowmelt across the TP were based on the simulations of albedo reduction and RF. It was found that glacial snowmelt water caused by LAPs contributed ~20 % of the total mass balance. These findings revealed that the effects of both BC and non-BC absorbers need to be properly accounted for in future regional climate projections, in particular on the high-altitude cryosphere.

Data availability

Black carbon and other light absorbing data are available upon request from Professor Shichang Kang and Dr. Yulan Zhang.

Author contribution

Y. Zhang, S. Kang, and Z. Cong designed the experiments. M. Sprenger performed the footprint simulations. Y. Zhang, T. Gao, C. Li, X. Li, X. Zhong, and M. Xu, carried out the experiments. S. Tao and W. Meng analyzed the black carbon inventory. M. Sillanpää and X. Qin gave valuable comments. Y. Zhang prepared the manuscript with contributions from all co-authors.

Acknowledgement

We acknowledge the support provided by the National Natural Science Foundation of China (41630754, 41671067, and 41421061), State Key Laboratory of Cryospheric Sciences (SKLCS-ZZ-2017), Chinese Academy of Sciences (KJZD-EW-

G03-04), the Foundation for Excellent Youth Scholars of the Northwest Institute of Eco-Environment and Resources, CAS, and the China Scholarship Council. We also thank Dr. M Flanner for help with simulating reflectance with the SNICAR model, and the reviewers who helped to improve this manuscript.

References

Andreae, M. O., and Gelencsér, A.: Black carbon or brown carbon? The nature of light-absorbing carbonaceous aerosols, Atmos. Chem. Phys., 6, 3131–3148, 2006.

Andreae, M. O., and Ramanathan, V.: Climate's dark forcings, Science, 340, 280−281, 2013.

Aoki, T., Aoki, T., Fukabori, M., Hachikubo, A., Tachibana, Y., Nishio, F.: Effects of snow physical parameters on spectral albedo and bidirectional reflectance of snow surface, J. Geophys. Res, 105(D8), 10219−10236, 2000.

Aoki, T., Matoba, S., Yamaguchi, S., Tanikawa, T., Niwano, M., Kuchiki, K., Adachi, K., Uetake, J., Motoyama, H., Hori, M.: Light-absorbing snow impurity concentrations measured on Northwest Greenland ice sheet in 2011 and 2012, Bull. Galciol. Res., 32, 21-31, doi:10.5331/bgr.32.21, 2014.

Aoki, T., Motoyoshi, H., Kodama, Y., Yasunari, T. J., Sugiura, K., Kobayashi, H.: Atmospheric aerosol deposition on snow surfaces and its effect on albedo, SOLA, 2013–2016, doi:10.2151/sola.2006-004, 2006.Bahadur, R., Praveen, P.S., Xu, Y., Ramanathan, V.: Solar absorption by elemental and brown carbon determined from spectral observation, Proc. Natl Acad. Sci. USA, 109(43), 17366–17371, doi: 10.1073/pnas.1205910109, 2012.

Bai, Y., and Feng, X.: Introduction to some research work on snow remote sensing, Remote Sens. Technol. Appl., 12(2), 59−65, 1994.

Beniston, M., Farinotti, D., Stoffel, M., Andreassen, L. M., Coppola, E., Eckert, N., Fantini, A., Giacona, F., Hauck, C., Huss, M., Huwald, H., Lehning, M., López-Moreno, J.-I., Magnusson, J., Marty, C., Moran-Tejéda, E., Morin, S., Naaim, M., Provenzale, A., Rabatel, A., Six, D., Stötter, J., Strasser, U., Terzago, S., Vincent, C.: The European mountain cryosphere: A review of past, current and future issues, Cryosphere Discuss., doi:10.5194/tc-2016-290, 2017.

Bond, T. C., Doherty, S. J., Fahey, D. W., Forster, P. M., Berntsen, T., DeAngelo, B. J., Flanner, M. G., Ghan, S., Kärcher, B., Koch, D., Kinne, S., Kondo, Y., Quinn, P. K., Sarofim, M. C., Schultz, M. G., Schultz, M., Venkataraman, C., Zhang, H., Zhang, S., Bellouin, N., Guttikunda, S.K., Hopke, P. K., Jacobson, M. Z., Kaiser, J. W., Klimont, Z., Lohmann, U., Schwarz, J. P., Shindell, D., Storelvmo, T., Warren, S. G., Zender, C. S.: Bounding the role of black carbon in the climate system: A scientific assessment, J. Geophys. Res. Atmos., 118, 5380–5552, doi:10.1002/jgrd.50171, 2013.

Brown, R. D. and Mote, P. W.: The response of northern Hemisphere snow cover ot a changing climate, J. Clim., 22, 2124–2145, doi: 10.1175/2008JCLI2665.5, 2009.

Cao, J., Lee, S. C., Ho, K. F., Zhang, X., Zou, S. C., Fung, K., Chow, J. C., Watson, J. G.: Characteristics of carbonaceous aerosol in Pearl River Delta Region, China during 2001 winter period, Atmos. Environ., 37:1451–1460, 2003.

Che, T., Dai, L., Wang, J., Zhao, K., Liu, Q.: Estimation of snow depth and snow water equivalent distribution using airborne microwave radiometry in the Binggou Watershed, the uppwe reaches of the Heihe River basin, Int. J. Appl. Earth Obs. Info., 17, 23–32, doi:10.1016/j.jag.2011.10.014, 2012.

Che, T., Li, X., Jin, R., Armstrong, R., Zhang, T.: Snow depth derived from passive microwave remote-sensing data in China, Ann. Glaciol., 49, 145–154, doi:10.3189/172756408787814690, 2008.

Chen, Y., and Bond, T.: Light absorption by organic carbon from wood combustion, Atmos. Chem. Phys., 10, 1773–1787, 2010.

Cheng, G. and Wu, T.: Responses of permafrost to climate change and their environmental significance, Qianhai-Tibet Plateau, J. Geophys. Res. Earth Surface, doi:10.1029/2006JF000631, 2007.

Chow, J. C., Watson, J. G., Chen, L.-W.A., Arnott, W.P., Moosmuller, H., Fung, K. K.: Equivalence of elemental carbon by Thermal/Optical Reflectance and Trsmittance with different temperature protocols, Environ. Sci. Technol., 38(16), 4414-4422, 2004.

Chýlek, P., Srivastava, V., Cahenzli, L., Pinnick, R. G., Dod, R. L., Novakov, T., Cook, T. L., Hinds, B. D.: Aerosol and graphitic carbon content of snow, J. Geophys. Res., 92, 9801-9809, 1987.

Cong, Z., Kang, S., Kawamura, K., Liu, B., Wan, X., Wang, Z., Gao, S., Fu, P.: Carbonaceous aerosols on the south edge of the Tibetan Plateau: concentrations, seasonality and sources, Atmos. Chem. Phys., 15, 1573-1584, 2015a.

Cong, Z., ., Kawamura, K., Kang, S., Fu, P.: Penetration of biomass-burning emissions from South Asia through the Himalayas: new insights from organic acids, Sci. Rep., 5, 9580, doi:10.1038/srep09580, 2015b.

Dang, C., Hegg, A.: Quantifying light absorption by organic carbon in Western North American snow by serial chemical extractions, J. Geophys. Res. Atmos., 119, 10247-10261, doi:10.1002/2014JD022156, 2014.

Di Mauro, B., Fava, F., Ferrero, L., Garzonio, R., Baccolo, G., Delmonte, B., Colombo, R.: Mineral dust impact on snow radiative properties in the European Alps combining ground, UAV, and satellite observations, J. Geophys. Res. Atmos., 120, 6080–6097, doi:10.1002/2015JD023287, 2015.

Di Mauro, B., Baccolo, G., Garzonio, R., Giardino, C., Massabò, D., Piazzalunga, A., Rossini, M., Colombo, R.: Impact of impurities and cryoconite on the optical properties of the Morteratsch glacier (Swiss Alps), Cryosphere Discuss., doi:10.5194/tc-2017-66, 2017.

Doherty, S. J., Dang, C., Hegg, D. A., Zhang, R., Warren, S. G.: Black carbon and other light-absorbing particles in snow of central North America, J. Geophys. Res. Atmos., 119, 12807-12831, doi:10.1002/2014JD022350, 2014.

Doherty,S. J., Hegg, D. A., Johnson, J. E., Quinn, P. K., Schwarz, J. P., Dang, C., Warren, S. G.: Causes of variability in light absorption by particles in snow at sites in Idaho and Utah, J. Geophys. Res. Atmos., 121(9), 4751−4768, 2016.

Doherty, S. J., Warren, S. G., Grenfell, T. C., Clarke, A. D., Brandt, R. E.: Light-absorbing impurities in Arctic snow, Atmos. Chem. Phys., 10, 11647-11680, doi:10.5194/acp-10-11647-2010, 2010.

Dumont, M., Brun, E., Picard, G., Libios, Q., Petit, J.-R., Geyer, M., Morin, S., Josse, B.: Contribution of light-absorbing impurities in snow to Greenland's darkening since 2009, Nat. Geosci., 7, doi:10.1038/NGEO2180, 2014.

Euskirchen, E. S., McGuire, A. D., Chapin III, F. S.: Energy feedbacks of northern high-latitude ecosystems to the climate system due to reduced snow cover during 20th century warming, Global Change Biol., 13, 2425-2438, doi:10.1111/j.1365-2486.2007.01450.x, 2007.

Flanner, M. G., Zender, C. S., Hess, P. G., Mahowald, N. M., Painter, T. H., Ramanathan, V., Rasch, P. J.: Springtime warming and reduced snow cover from carbonaceous particles, Atmos. Chem. Phys., 9, 2481–2497, 2009.

Flanner, M. G., Zender, C. S., Randerson, J. T., Rasch, P. J: Present-day climate forcing and response from black carbon in snow. J. Geophys. Res., 112, D11202, 2007.

Flanner, M. G.: Arctic climate sensitivity to local black carbon, J. Geophys. Res. Atmos., 118, 1840-1851, doi:10.1002/jgrd.50176, 2013.

Forsström, S., Isaksson, E., Skeie, R. B., Strom, J., Pedersen, C.A., Hudson, S.R., Berntsen, T. K., Lihavainen, H., Godtliebsen, F., Gerland, S.: Elemental carbon measurements in European Arctic snow packs, J. Geophys. Res. Atmos., 118, 13614–13627, doi:10.1002/2013JD019886, 2013

Gabbi, J., Huss, M., Bauder, A., Cao, F., Schwiowski, M.: The impact of Saharan dust and black carbon on albedo and long-term mass balance of an Alpine glacier, Cryosphere, 9, 1385-1400, 2015.

Gardner, A. S., Moholdt, G., Cogley, J. G., Wouters, B., Arendt, A. A., Wahr, J., Berthier, E., Hock, R., Pfeffer, W. T., Kaser, G., Ligtenberg, S. R. M., Bolch, T., Sharp, M. J., Hagen, J. O., van den Broeke, M. R., Paul, F.: A reconciled estimate of glacier contributions to sea level rise: 2003 to 2009, Science, 340, 852-858, 2013.

Gardner, A. S. and Sharp, M. J.: A review of snow and ice albedo and the development of a new physically based broadband albedo parameterization, J. Geophys. Res., 115, F01009, doi:10.1029/2009JF001444, 2010.

Gertler, C. G., Puppala, S. P., Panday, A., Stumm, D., Shea, J.: Black carbon and the Himalayan cryosphere: A review, Atom. Environ., 125, 404-417, doi: 10.1016/j.atmosenv.2015.08.078, 2016.

Ginot, P., Dumont, M., Lim, S., Patris, N., Taupin, J.-D., Wagnon, P., Gilbert, A., Arnaud, Y., Marinoni, A., Bonasoni, P., Laj, P.: A 10 year record of black carbon and dust from a Mera Peak ice core (Nepal): variability and potential impact on melting of Himalayan glaciers, Cryosphere, 8, 1479−1496, doi:10.5194/tc-8-1479-2014, 2014.

Grenfell, T. C., Warren, S. G., Mullen, P. C.: reflection of solar radiation by the Antarctic snow surface at ultraviolet, visible, and near-infrared wavelengths, J. Geophys. Res, 99(D9), 18669−18684, 1994.

Grenfell, T. C., and Warren, S. G.: Representation of a nonspherical ice particle by a collection of independent sphere for scattering and obsorption of radiation, J. Geophys. Res., 104(D24), 31697–31709, 1999.

Gustafsson, Ö., and Ramanathan, V.: Convergence on climate warming by black carbon, Proc. Natl. Acad. Sci. U.S.A., doi:10.1073/pnas.1603570113, 2016.

Hadley, O. L., Kirchstetter, T. W.: Black-carbon reduction of snow albedo, Nat. Clim. Chan., 2, doi:10.1038/NCLIMATE1433, 2012.

Hansen, J. and Nazarenko, L.: Soot climate forcing via snow and ice albedos, Proc. Natl Acad. Sci. USA, 101, 423–428, 2004.

Hao, X.: Retrieval of alpine snow cover area and grain size basing on optical remote sensing. PhD thesis, Cold and Arid Regions Environment Engineering Research Institute, Lanzhou, China, pp. 103–104, 2009.

He, C., Liou, K.-N., Takano, Y., Gu, Y., Qi, L., Mao, Y., Leung, L. R.: Black carbon radiative forcing over the Tibetan Plateau, Geophys. Res. Lett., 41, 7806–7813, doi:10.1029/2014GL062191, 2014.

Huang, J., Fu, Q., Zhang, W., Wang, X., Zhang, R., Ye, H., Warren, S. G.: Dust and black carbon in seasonal snow across northern China, BAMS, doi:10.1175/2010BAMS3064.1, 2011.

Immerzeel, W. W., van Beek, L. P. H., Bierkens, M. F. P.: Climate change will affect the Asian water towers, Science, 328, 1382–1385, 2010.

Jacobi, H.-W., Lim, S., Ménégoz, M., Ginot, P., Laj, P., Bonasoni, P., Stocchi, P., Marinponi, A., Araud, Y.: Black carbon in snow in the upper Himalayan Khumbu Valley, Nepal: observation and modelling of the impact on snow albedo, melting, and radiative forcing, Cryoshere, 9, 1385-1400, doi:10.5194-tc-1385-2015, 2015.

Ji, Z., Kang, S., Cong, Z., Zhang, Q., Yao, T.: Simulation of carbonaceous aerosols over the Third Pole and adjacent regions: distribution, transportation, deposition, and climatic effects, Clim. Dyn., doi:10.1007/s00382-015-2509-1, 2015.

Ji, Z., Kang, S., Zhang, Q., Cong, Z., Chen, P., Sillanpää, M.: Investigation of mineral aerosols radiative effects over Hihg Mountain Asia in 1990-2009 using a regional climate model, Atmos. Res., 178–179, 484–496, doi: 10.1016/j.atmosres.2016.05.003, 2016a.
Ji, Z.: Modeling black carbon and its potential radiative effects over the Tibetan Plateau, Adv. Clim. Change Res., 7, 139-144, 2016b.
Kang, S., Xu, Y., You, Q., Flühel, W.-A., Pepin, N., Yao, T.: Review of climate and cryosphere change in the Tibetan Plateau, Environ. Res. Lett., 5, 015101, doi:10.1088/1748-9326/5/1/015101, 2010.
Kaspari, S., Painter, T. H., Gysel, M., Skiles, S. M., Schwikowski, M.: Seasonal and elevational variations of black carbon and dust in snow and ice in the Solu-Khumbu, Nepal and estimated radiative forcings, Atmos. Chem. Phys., 14, 8089–8103, 2014.
Kokhanovsky, A. A., and Zege, E. P.: Scattering optics of snow, Appl. Optics, 43(7), 1589–1602, 2004.
Kopacz, M., Mauzerall, D. L., Wang, J., Leibensperger, E. M., Henze, D. K., Singh, K.: Origin and radiative forcing of black carbon transported to the Himalayas and Tibetan Plateau, Atmos. Chem. Phys., 11, 2837–2852, doi:10.5194/acp-11-2837-2011, 2011.
Kuchiki, K., Aoki, T., Niwano, M., Matoba, S., Kodama, Y., Adachi, K.: Elemental carbon, organic carbon, and dust concentrations in snow measured with thermal optical and gravimetric methods: Variations during the 2007-2013 winters at Sapporo, Japan, J. Geophys. Res. Atmos., 120, 868-882, doi:10.1002/2014JD022144, 2015.
Kuipers Munneke, P., Reijmer, C. H., van den Broeke, M. R., König-Langlo, G., Stammes, P., Knpa, W. H.: Analysis of clear-sky Antarctic snow albedo using observations and radiative transfer modelling, J. geophys. Res- Atmos., 113(D17118), doi:10.1029/2007JD009653, 2008.
Lau, W. K. M., Kim, M.-K., Kim, K.-M., Lee, W.-S.: Enhanced surface warming and accelerated snow melt in the Himalayas and Tibetan Plateau induced by absorbing aerosols, Environ. Res. Lett., 5, 025204, doi:10.1088/1748-9326/5/2/025204, 2010.
Li, C., Bosch, C., Kang, S., Andersson, A., Chen, P., Zhang, Q., Cong, Z., Chen, B., Qin, D., Gustafsson, Ö.: Sources of black carbon to the Himalayan-Tibetan Plateau glaciers, Nat. Comm., 7, 12574, doi:10.1038/ncomms12574, 2016.
Li, X., Kang, S., He, X., Qu, B., Tripathee, L., Jing, Z., Paudyal, R., Li, Y., Zhang, Y., Yan, F., Li, G., Li, C.: Light-absorbing impurities accelerate glacier melt in the Central Tibetan Plateau, Sci. Total Environ., doi:10.1016/j.scitotenv.2017.02.169, 2017.
Lin, G., Penner, J. E., Flanner, M. G., Sillman, S., Xu, L., Zhou, C.: radiative forcing of organic aerosol in the atmosphere and on snow: Effects of SOA and brown carbon, J. Geophys. Res. Atmos., 119, 7453-7476, doi:10.1002/2013JD021186, 2014.
Lu, Z., Streets, D. G., Zhang, Q., Wang, S.: A novel back-tracjectory analysis of the origin of black carbon transported to the Himalayas and Tibetan Plateau during 1996–2010, Geophys. Res. Lett., 39(L01809), doi:10.1029/2011GL049903, 2012.
Ma, L., Qin, D.: Temporal–spatial characteristics of observed key parameters of snow cover in China during 1957–2009, Sci. Cold Arid Reg., 4, 384–393, doi:10.3724/SP.J.1226.2012.00384, 2012.
Ménégoz, M., Krinner, G., Balkanski, Y., Boucher, O., Cozic, A., Lim, S., Ginot, P., Laj, P., Gallée, H., Wagnon, P., Marinoni, A., Jacobi, H. W.: Snow cover sensitivity to black carbon deposition in the Himalayas: from atmospheric and ice core measurements to regional climate simulations, Atmos. Chem. Phys., 14, 4237-4249, doi:10.5194/acp-14-4237-2014, 2014.
Menon, S., Koch, D., Beig, G., Shu, S., Fasullo, J., Orlikowski, D.: Black carbon aerosol and the third polar ice cap, Atmos. Chem. Phys., 10, 4559–4571, doi:10.5194/acp-10-4559-2010, 2010.
Ming, J., Xiao, C., Cachier, H., Qin, D., Qin, X., Li, Z., Pu, J.: Black carbon (BC) in the snow of glaciers in west China and its potential effects on albedos, Atmos. Res., 92, 114-123, doi: 10.1016/j.atmosres.2008.09.007, 2009.
Moosmüller, H., Engelbrecht, J. P., Skiba, M., Frey, G., Chakrabarty, P. K., Arnott, W. P.: Single scattering albedo of fine mineral dust aerosols controlled by iron concentration, Journal of Geophys. Res., 117(D11210), doi:10.1029/2011JD016909, 2012.
Mugnai, A., and Wiscombe, W. J.: Scattering of radiation by moderately nonspherical particles. J. Atmos. Sci., 37, 1291–1307, 1980.
Nechel, N., Kropáček, J., Bolch, T., Hochschild, V.: Glacier mass changes on the Tibetan Plateau 2003-2009 derived from ICESat laser altimetry measurements, Environ. Res. Lett., 9(1), 014009, doi: 10.1088/1748-9326/9/1/014009, 2014.
Niu, H., Kang, S., Shi, X., Paudyal, R., He, Y., Li, G., Wang, S., Pu, T., Shi, X.: In-situ measurements of light-absorbing impurities in snow of glacier on Mt. Yulong and implications for radiative forcing estimates, Sci. Total Environ., doi: 10.1016/j.scitotenv.2017.01.032, 2017.
Painter, T. H., Barrett, A. P., Landry, C. C., Neff, J. C., Cassidy, M. P., Lawrence, C. R., McBride, K. E., Farmer, G. L.: Impact of disturebed desert soils on duration of mountain snow cover, Geophys. Res. Lett., 34, L12502, doi:10.1029/2007GL030284, 2007.
Painter, T. H., Deems, J. S., Belnap, A. F., Landry, C. C., Udall, B.: Response of Colorado River runoff to dust radiative forcing in snow, Proc. Natl. Acad. Sci. USA, 107(40), 17125-17130, doi:10.1073/pnas.0913139107, 2010.
Painter, T. H., Seidel, F. C., Bryant, A. C., Skiles, S. M., Rittger, K.: Imaging spectroscopy of albedo and radiative forcing by light-absorbing impurities in mountain snow, J. Geophys. Res. Atmos., 118, 9511-9523, doi:10.1002/jgrd.50520, 2013.
Pu, Z., Xu, L., Salomonson, V. V.: MODIS/Terra observed seasonal variations of snow cover over the Tibetan Plateau, Geophys. Res. Lett., 34(L06706), doi:10.1029/2007GL029262, 2007.
Qian, Y., Flanner, M. G., Leung, L. R., Wang, W.: Sensitivity studies on the impacts of Tibetan Plateau snowpack pollution on the Asian hydrological cycle and monsoon climate, Atmos. Chem. Phys., 11, 1929–1948, doi:10.5194/acp-11-1929-2011, 2011.
Qian, Y., Wang, H., Zhang, R., Flanner, M. G., Rasch, P. J.: A sensitivity study on modelling black carbon in snow and its radiative forcing over the Arctic and northern China, Eviron. Res. Lett., 9, 064001, doi:10.1088/1748-9326/9/6/064001, 2014.

Qian, Y., Yasunari, T. J., Doherty, S. J., Flanner, M. G., Lau, W. K. M., Ming, J., Wang, H., Wang, M., Warren, S. G., Zhang, R.: Light-absorbing particles in snow and ice: measurement and modeling of climatic and hydrological impact, Adv. Atmos. Sci., 32, 64–91, doi: 10.1007/s00376-014-0010-0, 2015.

Qu, B., Ming, J., Kang, S., Zhang, G., Li Y., Li, C., Zhao, S., Ji, Z. and Cao, J.: The decreasing albedo of the Zhadang glacier on western Nyainqengtanglha and the role of light-absorbing impurities, Atmos. Chem. Phys., 14, 11117–11128, doi:10.5194/acp-14-11117-2014, 2014.

Ramanathan, V. and Carmichael, G.: Global and regional climate changes due to black carbon, Nat. Geosci., 1, 221-227, doi:10.1038/nego156, 2008.

Schmale, J., Flanner, M., Kang, S., Sprenger, M., Zhang, Q., Guo, J., Li, Y., Schwikowski, M., Farinotti, D.: Modulation of snow reflectance and snowmelt from Central Asian glaciers by anthropogenic black carbon, Sci. Rep., 7, 40501, doi:10.1038/srep40501, 2017.

Skiles, S. M. and Painter, T. H.: Daily evolution in dust and black carbon content, snow grain size, and snow albedo during snowmelt, Rocky Mountains, Colorado, J. Glaciol., doi:10.1017/jog.2016.125, 2016.

Skiles, S. M., Painter, T. H., Belnap, J., Holland, L., Reynolds, R. L., Goldstein, H. L., Lin, J.: Regional variability in dust-on-snow processes and impacts in the Upper Colorado River basin, Hydrol. Process., doi:10.1002/hyp.10569, 2015.

Sprenger, M., and Wernli, H.: The LAGRANTO Lagrangian analysis tool–version 2.0, Geosci. Model Dev., 8, 2569–2586, doi: 10.5194/gmd-8-2569-2015, 2015.

Tahir, A. A., Chevallier, P., Arnaud, Y., Ashraf, M., Bhatti, M. T.: Snow cover trend and hydrological characteristics of the Astore River basin (Western Himalayas) and its comparison to the Hunza basin (Karakoram region), Sci. Total Environ., 505, 748–761, doi: 10.1016/j.scitotenv.2014.10.065, 2015.

Toon, O. B., McKay, C. P., Ackerman, T. P., Santhanam, K.: Rapid calculation of radiative heating rates and photodissociation rates in inhomogeneous multiple scattering atmospheres, J. Geophys. Res. Atmos., 94(D13), 16287–16301, 1989.

Vernek, A. D., Zhou, J., Shukla, J.: The effect of Eurasian snow cover on the Indian Monsoon, J. Clim., 8, 248–266, 1995.

Voisin, D., Jaffrezo, J.-L., Houdier, S., Barret, M., Cozic, J., King, M. D., France, J. L., Reay, H. J., Grannas, A., Kos, G., Ariya, P. A., Beine, H. J., Domine, F.: Carbonaceous species and humic like substances (HULIS) in Arctic snowpack during OASIS field campaign in Barrow, J. Geophys. Res., 117(D00R19), doi:10.1029/2011JD016612, 2012.

Wang, M., Xu, B., Zhao, H., Cao, J., Joswiak, D., Wu, G., Lin, S.: The influence of dust on quantitative measurements of black carbon in ice and snow when using a thermal optical method, Aerosol Sci. Tech., 46:1, 60–69, doi:10.1080/02786826.2011.605815, 2012.

Wang, R., Tao, S., Shen, H., Huang, Y., Chen, H., Baljanski, Y., Boucher, O., Ciais, P., Shen, G., Li, W., Zhang, Y., Chen, Y., Lin, N., Su, S., Li, B., Liu, J., Liu, W.: Trend in black carbon emissions from 1960 to 2007, Environ. Sci. Technol., doi:10.1021/es5021422, 2014.

Wang, X., Doherty, S., Huang, J.: Black carbon and other light-absorbing impurities in snow across Northern China, J. Geophys. Res. Atmos., 118, 1471-1492, doi:10.1029/2012JD018291, 2013.

Warren, S. G., Clarke, A. D.: Soot in the atmosphere and snow surface of Antarctica, J. Geophys. Res., 95(D2), 1811-1816, 1990.

Wiedinmyer, C., Akagi, S. K., Yokelson, R. J., Emmons, L. K., Al-Saadi, J. A.: The Fire Inventory from NCAR (FINN): A high resolution global model to estimate the emissions from open burning, Geosci. Model Dev., 4, 625-641, doi:10.5194/gmd-4-625-2011, 2011.

Wu, G., Xu, T., Zhang, X., Zhang, C., Yan, N.: The visible spectroscopy of iron oxide minerals in dust particles from ice cores on the Tibetan Plateau, Tellus B, 68, 29191, doi: 10.3402/tellusb.v68.29191, 2016.

Xi, X. and Sokolik, I. N.: Dust interannual variability and trend in Central Asia from 2000 to 2014, and their climatic linkages, J. Geophys. Res. Atmos., 120, 12175–12197, doi:10.1002/2015JD024092, 2015.

Xiao, Z., and Duan, A.: Impacts of Tibetan Plateau snow cover on the interannual variability of the East Asian summer monsoon, J. Clim., 29, 8495−8514, doi:10.1175/JCLI-D-16-0029.1, 2016.

Xu, B., Cao, J., Hansen, J., Yao, T., Joswia, D. R., Wang, N., Wu, G., Wang, M., Zhao, H., Yang, W., Liu, X., He, J.: Black soot and the survival of Tibetan glaciers, Proc. Natl. Acad. Sci. U.S.A., 106 (52), 22114–22118, doi:10.1073/pnas.0910444106, 2009.

Xu, W., Ma, L., Ma, M., Zhang, H., Yuan, W.: Spatial-Temperal variability of snow cover and depth in the Qinghai-Tibetan Plateau, J. Clim., 30, 1521−1533, doi:10.1175/JCLI-D-15-0732.1, 2017.

Yan, F., Kang, S., Li, C., Zhang, Y., Qin, X., Li, Y., Zhang, X., Hu, Z., Chen, P., Li, X., Qu, B., Sillanpää, M.: Concentration, sources and light absorption characteristics of dissolved organic carbon on a medium-sized valley glacier, northern Tibetan Plateau, The Cryosphere, 10, 2611−2621, doi:10.5194/tc-10-2611-2016, 2016.

Yanai, M. and Wu, G.: Effects of the Tibetan Plateau, in B. Wang (ed.) The Asian Monsoon, Springer Berlin Heidelberg, 513-549, 2006.

Yang, S., Xu, B., Cao, J., Zender, C. S., Wang, M.: Climate effect of black carbon aerosol in a Tibetan Plateau glacier, Atmos. Environ., 111, 71-78, doi:10.1016/j.atmosenv.2015.03.016, 2015.

Yao, T., Masson-Delmotte, V., Gao, J., Yu, W., Yang, X., Risi, C., Sturm, C., Werner, M., Zhao, H., He, Y., Ren, W., Tian, L., Shi, C., Hou, S.: A review of climatic controls on $\delta^{18}O$ in precipitation over the Tibetan Plateau: Observations and simulations, Rev. Geophys., 51, doi:8755-1209/13/10.1002/rog.20023, 2013.

Yao, T., Thompson, L.G., Mosbrugger, V., Zhang, F., Ma, Y., Luo, T., Xu, B., Yang, X., Joswiak, D. R., Wang, W., Joswiak, M. E., Devkota, L. P., Tayal, S., Jilani, R., Fayziev, R.: Third Pole Environment (TPE), Environ. Development, 3, 52–64, doi: 10.1016/j.envdev.2012.04.002, 2012a.

Yao, T., Thompson, L.G., Yang, W., Yu, W., Gao, Y., Guo, X., Yang, X., Duan, K., Zhao, H., Xu, B., Pu, J., Lu, A., Xiang, Y., Kattel, D.B., Joswiak, D.: Different glacier status with circulations in TP and surroundings, Nat. Clim. Change, doi: 10.1038/NCLIMATE1580, 2012b.

Yasunari, T. J., Bonasoni, P., Laj, P., Fujita, K., Vuillermoz, E., Marinoni, A., Cristofanelli, P., Duchi, R., Tartari, G., Lau, K.-M.: Estimated impact of black carbon deposition during pre-monsoon season from Nepal Climate Observatory- Pyramid data and snow albedo changes over Himalayn glacier, Atmos. Chem. Phys., 10, 6603–6615, doi:10.5194/acp-10-6603-2010, 2010

Yasunari, T. J., Koster, R. D., Lau, Kim, K.-M.: Impact of snow darkening via dust, black carbon, and organic carbon on boreal spring climate in the Earth system, J. Geophys. Res. Atmos., 120, 5485-5503, doi:10.1002/2014JD022977, 2015.

Yasunari, T. J.,Tan, Q., Lau, K.-M., Bonasoni, P., Marinoni, A., Laj, P., Ménégoz, M., Takemura, T., Chin, M.: Estimated range of black carbon dry deposition and the related snow albedo reduction over Himalayan glaciers during dry pre-monsoon periods, Atom. Environ., 78, 259-267, doi: 10.1016/j.atmosenv.2012.03.031, 2013.

Ye, H., Zhang, R., Shi, J., Huang, J., Warren, S. G., Fu, Q.: Black carbon in seasonal snow across northern Xinjiang in northwestern China, Environ. Res. Lett., 7, 044002, doi:10.1088/1748-9326/7/4/04002, 2012.

Yuan, W., Xu, W., Ma, M., Chen, S., Liu, W., Cui, L.: Improved snow cover model in terrestrial ecosystem models over the Qinghai-Tibetan Plateau, Agr. Forest Meterol., 218–219, 161–170, doi: 10.1016/j.agrformet.2015.12.004, 2016.

Zatko, M. C., Grenfell, T. C., Alexander, B., Doherty, S. J., Thomas, J. L., Yang, X.: The influence of snow grain size and impurities on the vertical profiles of actinic flux and associated NOx emission on the Antarctic and Greenland ice sheets, Atmos. Chem. Phys., 13, 3547-3567, doi:10.5194/acp-13-3547-2013, 2013.

Zatko, M. C., Erbland, J., Savarino, J., Geng, L., Easley, L., Schauer, A. J., Bates, T. S., Quinn, P., Light, B., Morison, D., Osthoff, H. D., Lyman, S., Neff, W., Yuan, B., Alexander, B.: The magnitude of the snow-sourced reactive nitrogen flux to the boundary layer in the Uintah Basin, Utah, USA, Atmos. Chem. Phys., 16, 13537-13851, doi:10.5194/acp-16-13837, 2016.

Zeeman, M. J., Mauder, M., Steinbrecher, R., heidbach, K., Echart, E., Schmid, H. P.: Reduced snow cover ffects productivity of upland temperate grasslands, Agr. Forest Meterol., 232, 514–526, doi: 10.1016/j.agrformet.2016.09.002, 2017.

Zhang, R., Wang, H., Qian, Y., Rasch, P. J., Easter, R. C., Ma, P.-L., Singh, B., Huang, J., Fu, Q.: Quantifying sources, transport, deposition, and radiative forcing of black carbon over the Himalayas and Tibetan Plateau, Atmos. Chem. Phys., 15, 6205-6223, doi:10.5194/acp-15-6205-2015, 2015.

Zhang, X., Wu, G., Zhang, C., Xu, T., Zhou, Q.: What is the real role of iron oxides in the optical properties of dust aerosols? Atmos. Chem. Phys., 15, 12159–12177, 2015.

Zhang, Y., Kang, S., Zhang, Q., Gao, T., Guo, J., Grigholm, B., Huang, J., Sillanpää, M., Li, X., Du, W., Li, Y., Ge, X.: Chemical records in snowpits from high altitude glaciers in the Tibetan Plateau and its surroundings, PLoS ONE, 11(5), e0155232, doi:10.1371/journal.pone.0155232, 2016.

Zhang, Y., Kang, S., Cong, Z., Schmale, J., Sprenger, M., Li, C., Yang, W., Gao, T., Sillanpää, M., Li, X., Liu, Y., Chen, P., Zhang, X.: Light-absorbing impurities enhance glacier albedo reduction in the southeastern Tibetan Plateau, J. Geophys. Res. Atmos., 122, doi:10.1002/2016JD026397, 2017.

Zhang, Y., Li, T., Wang, B.: Decadal change of the spring snow depth over the Tibetan Plateau: The associated circulation and influence on the east Asian summer monsoon, J. Clim., 17, 2780-2793, 2004.

Zhao, H., and Moore, G.W.K.: On the relationship betwwn Tibetan snow cover, the Tibatan Plateau monsoon and the Indian summer monsoon, Geophys. Res. Lett., 31(L14204), doi:10.1029/2004GL020040, 2004.

Zhong, X., Zhang, T., Zheng, L., Hu, Y., Wang, H., Kang, S.: Spatiotemporal variability of snow depth across the Eurasian continent from 1966 to 2012, Cryosphere Discuss., doi:10.5194/tc-2016-182, 2016.

Zhou, L., Dickinson, R. E., Tian, Y., Zeng, X., Dai, Y., Yang, Z.-L., Schaaf, C. B., Gao, F., Jin, Y., Strahler, A., Myneni, R. B., Yu, H., Wu, W., Shaikh, M.: Comparison of seasonal and spatial variations of albedos from Moderate-Resolution Imaging Spectradiomater (MODIS) and Common Land Model, J. Geophys. Res, 108(D15), doi:10.1029/JD003326, 2003.

Table 1 Snow effective grain sizes and snow density used for the albedo calculation with the SNICAR model.

Description	Low scenario	Central scenario	High scenario
Snow effective grain radius (μm)	150	500	1500
Snow density (kg m^{-3})	150	250	400

Table 2 Summary of BC, OC and dust concentrations in snow over the Tibetan Plateau and other regions.

Sites	BC (ng g^{-1})	Dust (μg g^{-1})	OC (ng g^{-1})	OC/BC	Method	References
Southern TP (Region I)	1423±242	119.8±18.97	2145±325	1.82±0.17	DRI	This study
Central TP (Region II)	5624±1500	295±67.50	6119±1257	1.31±0.19	DRI	This study
Northern TP (Region III)	1484±626	93.20±27.05	974±197	1.14±0.15	DRI	This study
Himalayan Khumbu Valley	0.1-70				SP2	Jacobi et al., 2015
Himalayas	24.3±20.1	1.32±0.84	359±185.2	~10	Sunset	Lim et al., 2014
Qilian mountain	1550				ISSW	Wang et al., 2013
Border of Siberia, China	117				ISSW	Wang et al., 2013
Northeast China	1220				ISSW	Wang et al., 2013
Inner Mongolia, China	340				ISSW	Wang et al., 2013
Northwest China	10-150				ISSW	Pu et al., 2016
Sapporo, Japan	7-2800	10-1300	0.14-260		Sunset	Kuchiki et al., 2015
Central North America	5-70				ISSW	Doherty et al., 2014
Uintah basin, Utah, USA	5-100				ISSW	Zatko et al., 2016
Sierra Nevada, North America	11±7.7				DRI	Hadley et al., 2010
French Alps	4.3±4.5	3.06±5.25	59.6±77.6		SP2	Lim et al., 2014
Greenland Summit	3.1±1.4	0.262±0.117	142.6±82.6		SP2	Lim et al., 2014
Greenland	Sumit station: 1.4				ISSW	Zatko et al., 2013
Arctic	Scandinavia: 88 Svalbard: 11-14 Fram Strait: 7-42 Barrow: 9				Sunset	Forsström et al., 2013
Antarctic	Near Dome C: 2.1 Far from Dome C: 0.6				ISSW	Zatko et al., 2013

Note:

(1) DRI-DRI 2001A model thermal-optical carbon analysis

(2) SP2: Single Particle Soot Photometer

(3) ISSW- ISSW spectrophotometer

(4) Sunset: Sunset Lab OC-EC Aerosol Analyzer

Table 3 Comparison between measured albedo by ASD and simulated albedo (SA) by the SNICAR model.

Selected site (24K)	SA clean snow	SA BC	SA Dust	SA BC+Dust
SNICAR: Broadband (305-4495 nm)	0.7824	0.7027	0.7511	0.6892
SNICAR: Wavelength (350-2500 nm)	0.7728	0.6985	0.7453	0.6864
ASD measurement (350-2500 nm)		0.6709±0.0019		

Table 4 Simulated albedo (SA) and radiative forcing (RF) by BC and dust in snow cover across the Tibetan Plateau.

Different scenarios	SA clean snow	SA BC	SA Dust	SA BC+Dust	Contribution to albedo reduction	RF BC	RF Dust	RF BC+Dust
Low	0.7751±0.0193	0.6517±0.0702	0.7387±0.0250	0.6413±0.0710	37 %	16.32±0.0931	4.78±0.0310	17.64±0.0952
Medium	0.6943±0.0313	0.5104±0.0900	0.6372±0.0382	0.4992±0.0900	39 %	24.20±0.1250	7.57±0.0483	25.86±0.1233
High	0.5992±0.0435	0.3683±0.0935	0.5197±0.0490	0.3582±0.0889	38 %	30.96±0.1362	10.70±0.0653	32.36±0.1315

Table 5 Average reductions of snow cover duration by BC and dust for different short wavelengths (220, 270, and 310 W m^{-2}, respectively) and snow cover depth water equivalent (mm).

SD / Shortwave	SD=40 mm			SD=100 mm		
	BC	Dust	BC+dust	BC	Dust	BC+dust
SW=220 W m^{-2}	1.69±0.07	0.74±0.04	1.77±0.07	4.24±0.18	1.84±0.10	4.43±0.18
SW=270 W m^{-2}	1.38±0.06	0.60±0.03	1.44±0.06	3.45±0.15	1.50±0.08	3.61±0.15
SW=310 W m^{-2}	1.20±0.05	0.52±0.03	1.26±0.05	3.01±0.13	1.31±0.07	3.14±0.13

Figure 1

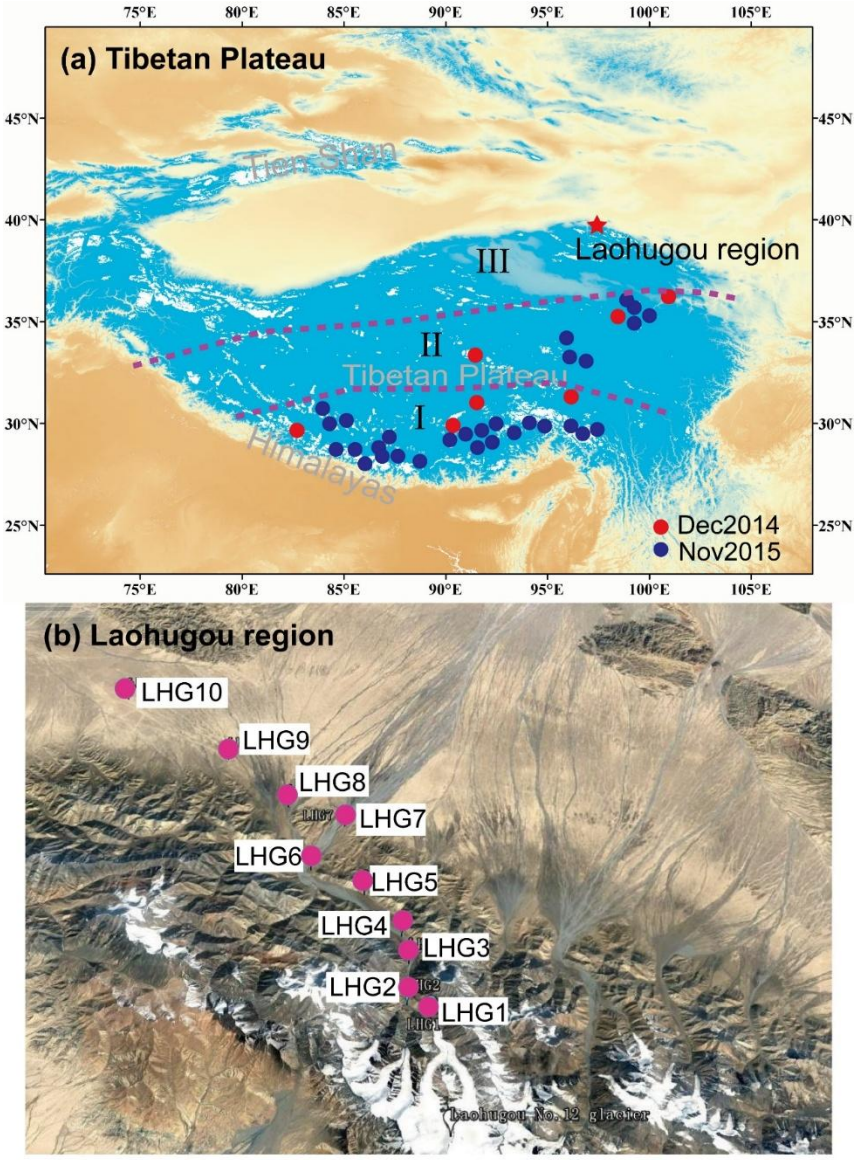

Figure 1: Snow sampling sites over (a) the Tibetan Plateau and (b) the Laohugou region.

Figure 2

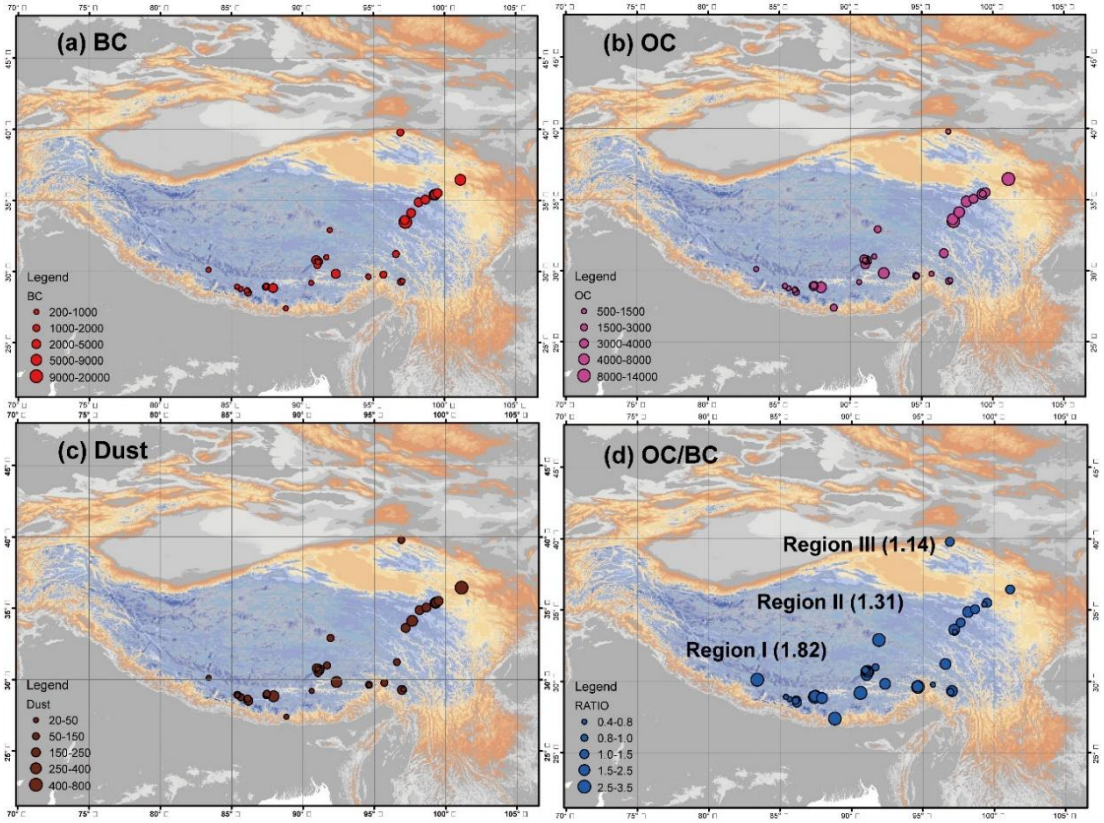

Figure 2: Spatial distributions of light-absorbing impurities in snow cover for each sampling site over the Tibetan Plateau. (a) BC, (b) OC, (c) Dust, and (d) ratio of OC to BC (OC/BC).

Figure 3

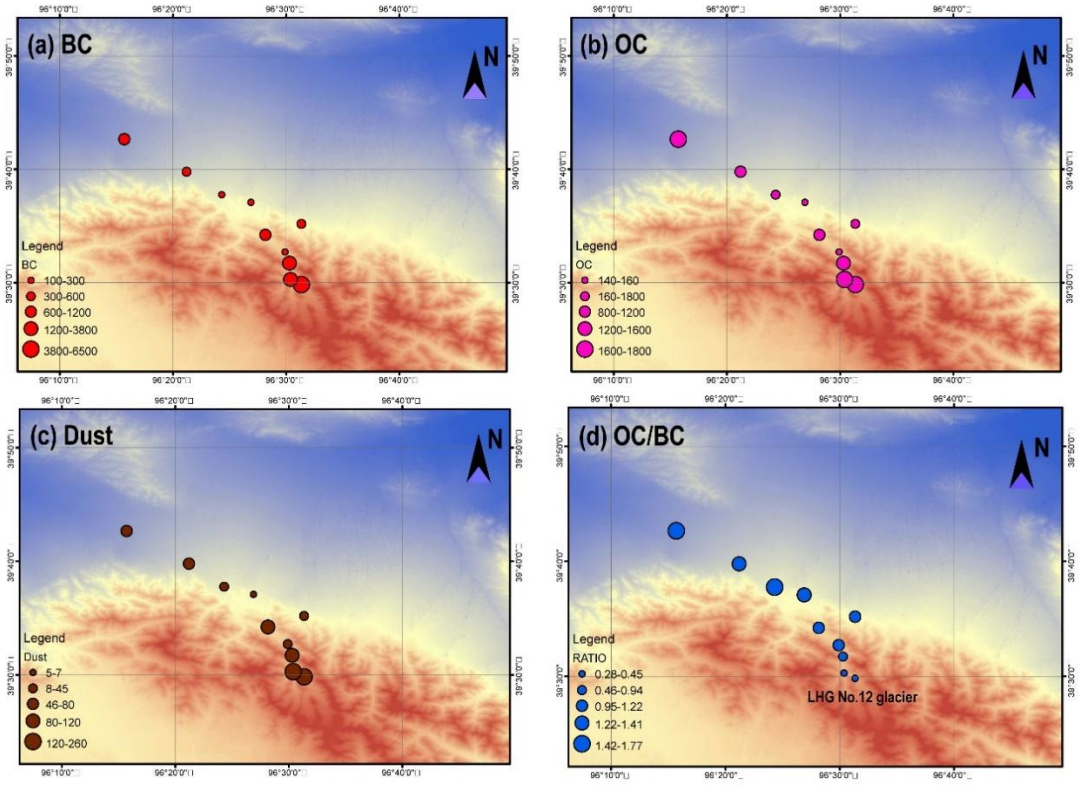

Figure 3. Spatial distributions of light-absorbing impurities in snow at the Laohugou region. (a) BC, (b) OC, (c) Dust, and (d) ratio of OC to BC (OC/BC).

Figure 4

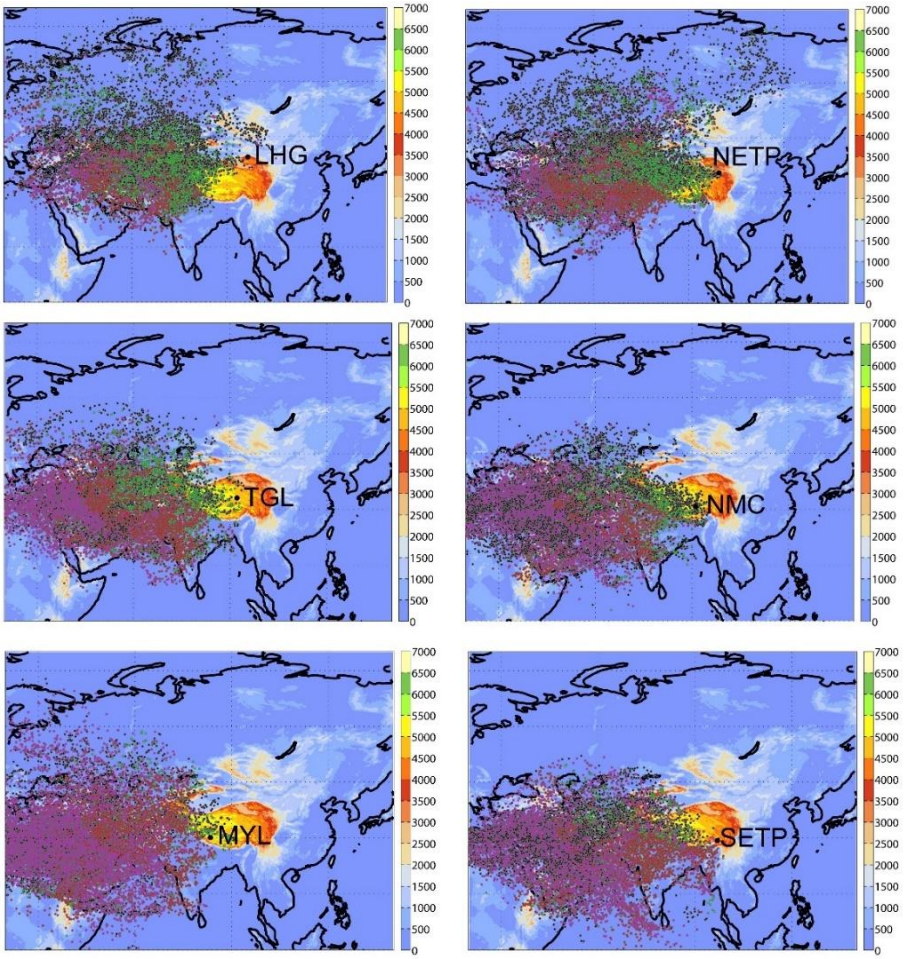

Figure 4: Footprint analyses for six selected sites over the Tibetan Plateau during the winter season (Nov 2015-Feb 2016). LHG and NETP in the northern Tibetan Plateau (Region III), TGL and NMC in the central Tibetan Plateau (Region II), and MYL and SETP in the southern Tibetan Plateau (Region I). (The right color bar means the height (m a.s.l.). The trajectories starting below 500 hPa were taken into account. Black dots: the air parcel did not pass near a fire during the 96 h prior to arrival at the studied site; Green dots: the air parcel did pass by a fire between -96 h and -48 h, but not afterwards, i.e., the 'contact' to a fire lies back at least 48 h before the air parcel arrived at Renlongba glacier; Magenta dots: contact with fires occurred between -48 h and 0 h before arriving at site; Red dots: contact with a fire before and after -48 h.)

Figure 5

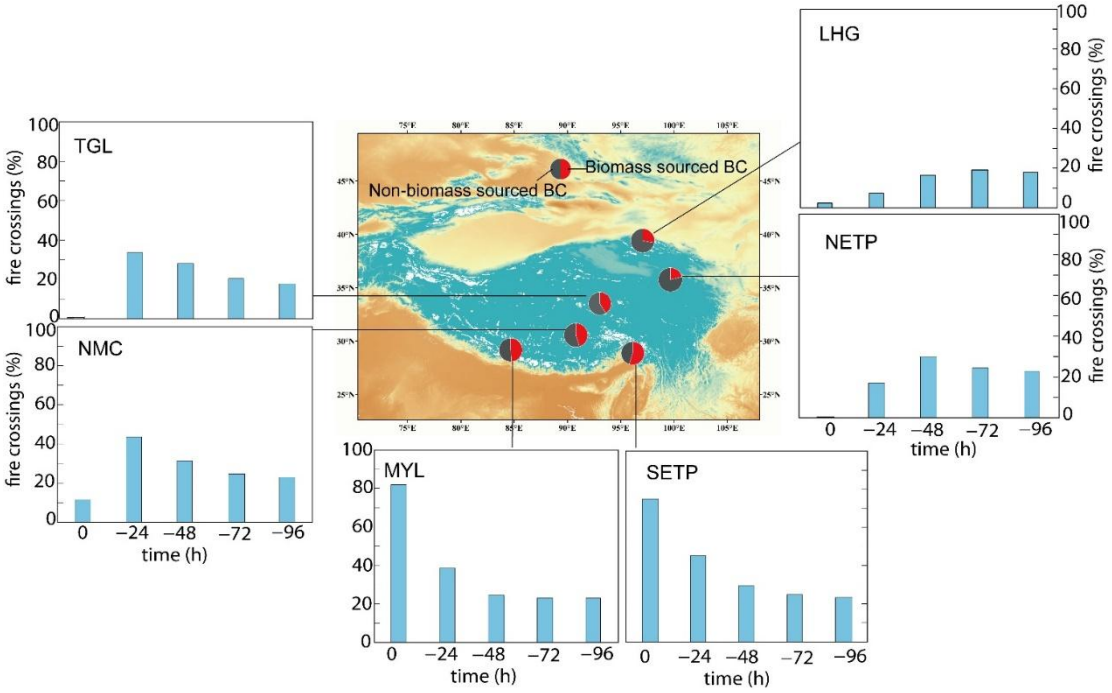

Figure 5: Different source contributions to BC deposition on the snow cover of the Tibetan Plateau.

Figure 6

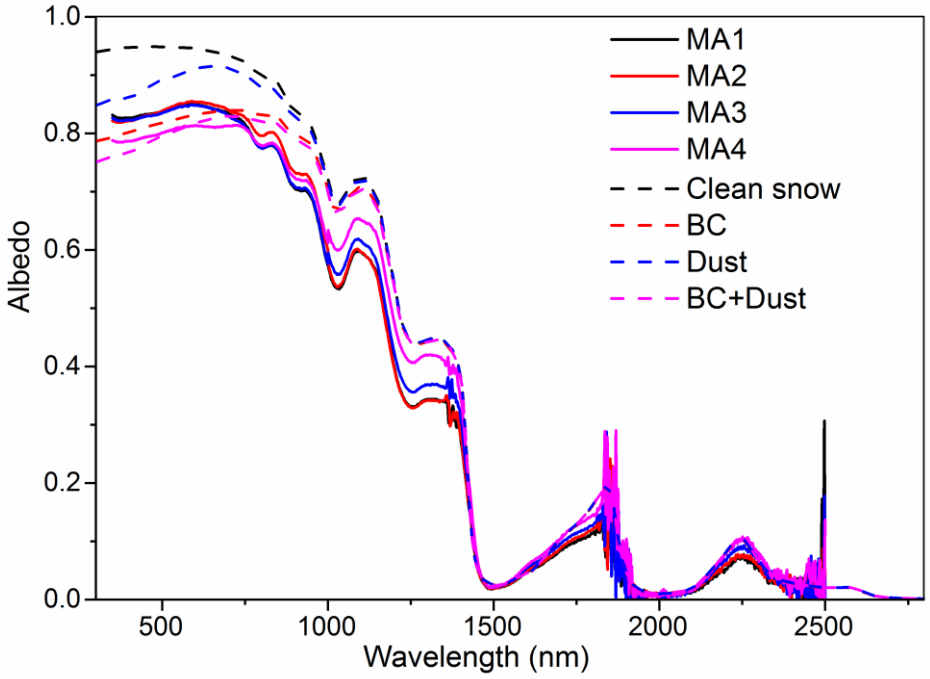

Figure 6: **Measured albedo by ASD (solid lines, MA1-4) and simulated effects of BC and dust on albedo (dashed lines) at the selected snow site on the Tibetan Plateau.**

Figure 7

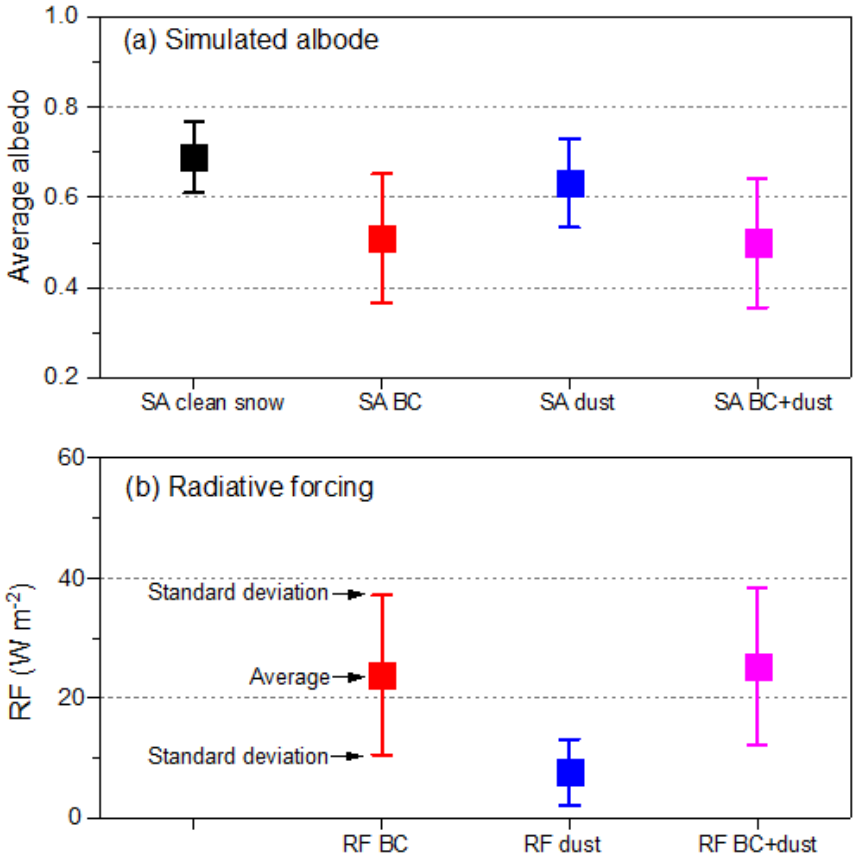

Figure 7: (a) Average albedo (solid rectangles) of snow cover due to aging only and impurities relative to the clean snow and (b) resulting clear sky instantaneous radiative forcing (solid rectangle means the average). (Note: SA means simulated albedo, SA BC means albedo only with BC in snow, SA dust means albedo only with dust in snow, and SA BC+dust means albedo with BC and dust in snow. RF means radiative forcing, RF BC means the RF caused by BC in snow, RF dust means the RF caused by dust in snow, and RF BC+dust means the RF caused by BC and dust in snow.The solid rectangles are the central average estimate whereas the bars show the standard deviation range of albedo and RF)

Figure 8

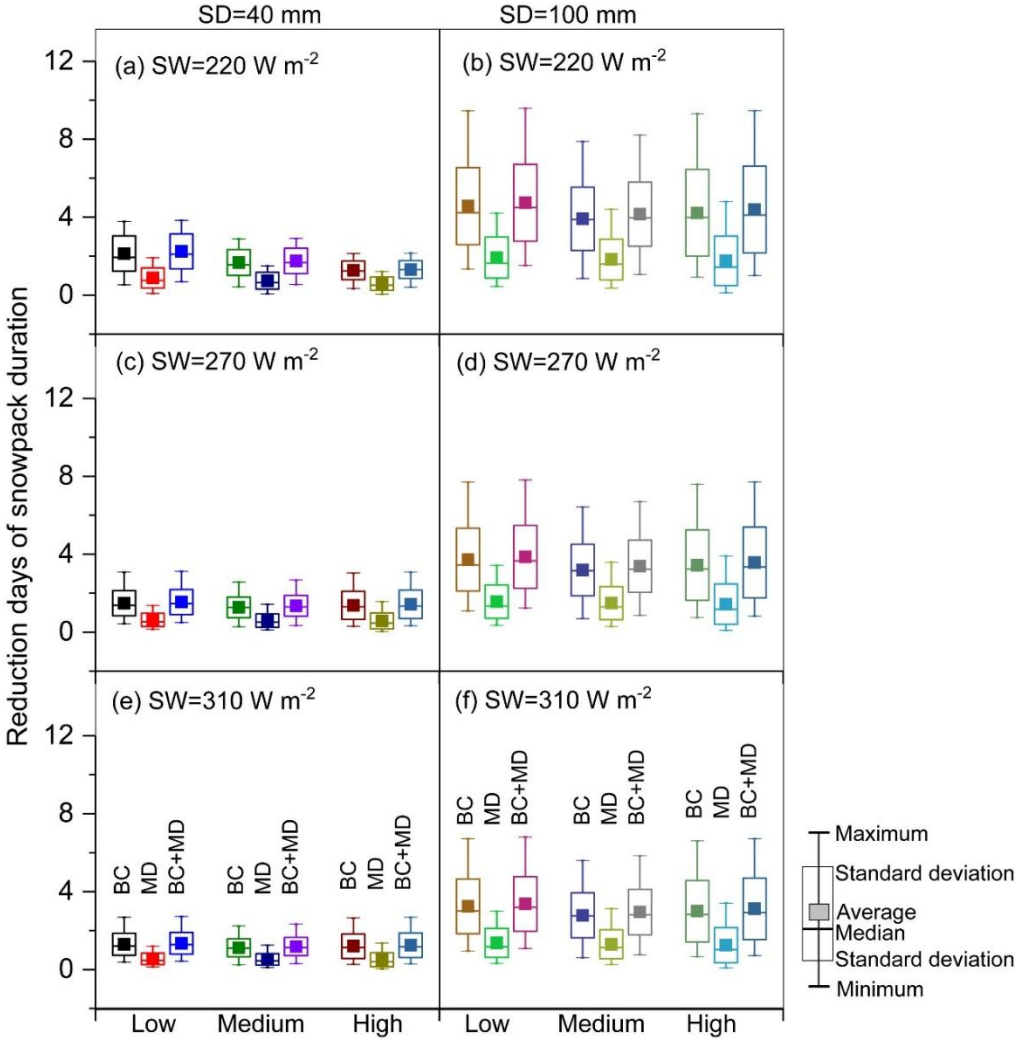

Figure 8: Reduction in days of snow cover duration by BC and dust for low, medium and high scenarios due to albedo reduction at different snow depth (SD=40 and 100 mm, respectively). a and b were simulated based on the daily shortwave at 220 W m-2. c and d were simulated based on the daily shortwave at 270 W m-2, e and f were simulated based on the daily shortwave at 310 W m-2. (Solid rectangles are average values; solid line in the box means the median; outliers of boxes are the one standard deviations of the average; and the bars are maximum and minimum values.)

Figure 9

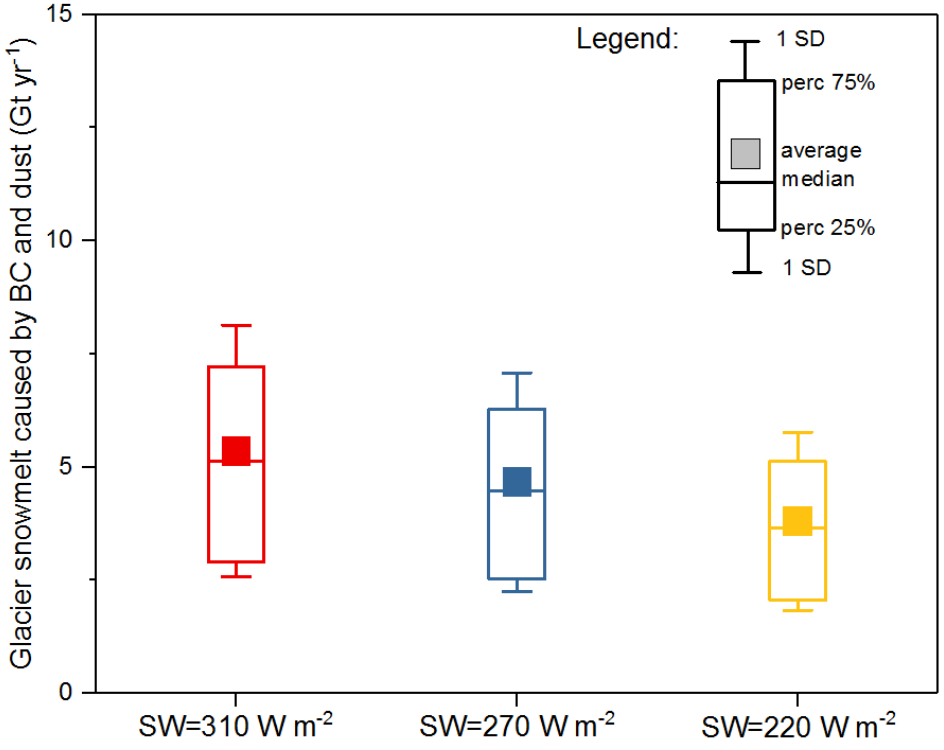

Figure 9: Estimates of total glacial snowmelt based on daily snowmelt caused by BC and dust for shortwave radiation at 220, 270, and 310 W m^{-2}, respectively. The days of daily temperature above 0 °C value is 100 (±25 %).

Supplementary materials for:

Black carbon and mineral dust in snow cover on the Tibetan Plateau

Yulan Zhang[1], Shichang Kang[1,2*], Michael Sprenger[3], Zhiyuan Cong[2], Tanguang Gao[4], Chaoliu Li[2], Shu Tao[5], Xiaofei Li[1], Xinyue Zhong[1], Min Xu[1], Wenjun Meng[5], Xiang Qin[1], Mika Sillanpää[6]

[1]State key laboratory of Cryospheric Science, Northwest Institute of Eco-Environment and Resources, Chinese Academy of Sciences, Lanzhou730000, China

[2]CAS Center for Excellence in Tibetan Plateau Earth Sciences, Beijing 100101, China

[3]Institute for Atmospheric and Climate Science, ETH Zurich, CH-8092 Zurich, Switzerland

[4]Key Laboratory of Western China's Environmental System (Ministry of Education), College of Earth and Environmental Sciences, Lanzhou University, Lanzhou 730000, China

[5]Department of Environmental Science, Laboratory for Earth Surface Processes, Peking University, Beijing, China

[6]Laboratory of Green Chemistry, Lappeenranta University of Technology, Mikkeli 50130, Finland

Correspondence to: Prof. Shichang Kang (shichang.kang@lzb.ac.cn)

Including:

Supplementary Tables S1-S3

Supplementary Figure S1-S5

Supplementary Tables

Table S1. Sampling information for snow cover over the Tibetan Plateau.

Table S2. Parameters for sensitivity analysis with SNICAR model for snow cover in the Tibetan Plateau. 1-Incident radiation (a. Direct, b. Diffuse); 2- Solar zenith angle; 3- Surface spectral distribution (a. Mid-latitude winter, clear-sky, cloud amount<5. b. Mid-latitude winter, cloudy, cloud amount ≥5); 4- Snow grain effective radius (μm); 5- Snowpack thickness (m); 6- Snowpack density (kg m^{-3}); 7- Albedo of underlying ground (a. Visible, 0.3–0.7μm, b. Near-infrared, 0.7–5.0μm); 8-MAC scaling factor (experimental) for BC; 9-BC concentration (ppb, sulfate-coated); 10- Dust concentration (μg g^{-1}, 5.0–10.0 μm diameter); 11- Volcanic ash concentration (ppm); 12- Experimental particle 1 concentration (ng g^{-1}).

Table S3. Short-wave radiation input data at selected sites across the Tibetan Plateau close to the snow sampling sites.

Table S1. Sampling information for snow cover over the Tibetan Plateau regions.

Sites	Time	Lat. (°)	Long. (°)	Elevation (m)	Snow depth (cm)	Density (kg m^{-3})	Observed snow grain size (μm)	Snow type	Snow temperature (°C)
LHG	2015-12-29 12:00	39.50	96.52	4250	20				
RYS	2014-12-03 12:25	36.50	101.52	3396					
TP-S-1511-36	2015-11-30 16:48	35.44	98.65	4363	11	300	2000	Coarse firn with hoar	–6.5
TP-S-1511-37	2015-11-30 18:10	35.37	99.29	4297	16	250	2000	Coarse firn with wind crust and dirty layer	–7.0
TP-S-1511-38	2015-12-01 10:09	35.39	99.31	4298	18	225	2000		–15.0
TP-S-1511-39	2015-12-01 11:23	35.51	99.51	4405	14	225	2000	Coarse firn	–6.5
TP-S-1511-35	2015-11-30 13:25	34.11	97.65	4781	10	325	2000	Coarse firn with dirty layer	–5.0
MD	2014-12-03 12:10	34.86	98.17	4220					
TP-S-1511-33	2015-11-30 11:12	33.47	97.24	4259	7	225	1000	Coarse firn	–4
TP-S-1511-34	2015-11-30 11:41	33.61	97.24	4366	12	350	2000	Coarse firn with wind crust	–6.0
TGL	2014-12-10 12:40	32.90	91.92	5163					
LWQ	2014-12-04 12:20	31.22	96.57	4370					
24K	2014-12-06 12:47	30.99	91.68	5100					
NMC	2014-12-09 12:30	30.75	91.68	4729					
MYL	2014-12-10 12:30	30.11	83.39	4610					
TP-S-1511-1	2015-11-15 11:30	30.45	91.05	4216	3		200	Firn	–5.0
TP-S-1511-2	2015-11-15 13:33	30.67	91.10	5036	6.8		1000	Firn	–3.7
TP-S-1511-3	2015-11-15 14:00	30.68	91.10	5124	9		1000	Fine firn	–0.14
TP-S-1511-4	2015-11-15 16:44	30.79	90.96	4687	5		1000	Fine firn	–2
TP-S-1511-5	2015-11-15 17:30	30.68	91.10	5096	17.1		500	Firn with wind crust	–4.8
TP-S-1511-6	2015-11-16 13:52	29.19	90.62	4762	6.8		1000	Firn	–3.7
TP-S-1511-16	2015-11-20 09:13	29.00	87.47	4798	9	300	1000	Fine firn	–17
TP-S-1511-27	2015-11-26 12:37	29.83	92.34	4971	17	150	3500	Coarse firn	–5
TP-S-1511-28	2015-11-27 10:55	29.63	94.63	4304	12	200	2000		–1.5
TP-S-1511-29	2015-11-27 11:25	29.61	94.67	4523	24	200	3000	Hoar at the bottom	–4.5
TP-S-1511-30	2015-11-27 17:48	29.77	95.70	3728	11	400	2000		–1.5
TP-S-1511-31	2015-11-28 12:10	29.26	96.94	4582	12	250	2000	Coarse firn, ice at bottom	–0.05
TP-S-1511-32	2015-11-28 1:45	29.32	97.03	4745	20	175	2000	Fresh snow and firn	–1.0
TP-S-1511-9	2015-11-18 12:13	28.82	87.93	4851	12.5	230	1500	Firn with wind crust and dirty layer	–12.6
TP-S-1511-17	2015-11-20 10:02	28.96	87.44	5163	15	270	2000	Firn with wind crust and dirty layer	–17
TP-S-1511-18	2015-11-20 10:35	28.91	87.43	5042	8	250	3000	Firn with wind crust and dirty layer	–15
TP-S-1511-21	2015-11-21 13:13	28.67	86.13	4565	9	200	2000	Coarse firn	–2.0
TP-S-1511-22	2015-11-21 14:09	28.52	86.17	5096	5	200	2000	Coarse firn	0
TP-S-1511-23	2015-11-22 13:12	28.65	86.08	4592	9	325	3000	Coarse firn with wind crust and hoar	
TP-S-1511-24	2015-11-22 14:11	28.76	85.66	4614	14	250	3000	Coarse firn	0.05
TP-S-1511-25	2015-11-22 15:07	28.90	85.40	4861	11.5	225	3000	Coarse firn	–2.5
TP-S-1511-26	2015-11-22 15:55	28.93	85.40	5166	12	275	1000	Fine firn with wind crust	0
TP-S-1511-8	2015-11-17 13:02	27.39	88.83	4150	5	275	1000	Fine firn	–0.4

Table S2. Parameters for sensitivity analysis with SNICAR model for snow cover in the Tibetan Plateau.

Site	1	2	3	4	5	6	7a	7b	8	9-BC	10-Dust	11	12
LHG*	direct	62.75	a		20		0.15	0.3	1	3745.46	224.49	0	0
RYS	direct	58.58	a		11		0.15	0.3	1	8922.53	417.65	0	0
TP-S-1511-36	direct	57.02	a		11		0.15	0.3	1	3097.59	172.04	0	0
TP-S-1511-37	direct	56.95	a		16		0.15	0.3	1	7373.45	292.97	0	0
TP-S-1511-38	direct	57.13	a		18		0.15	0.3	1	4122.43	233.86	0	0
TP-S-1511-39	direct	57.25	a		14		0.15	0.3	1	2894.96	157.78	0	0
TP-S-1511-35	direct	55.69	a		10		0.15	0.3	1	4217.19	295.80	0	0
MD	direct	56.94	a		11		0.15	0.3	1	3122.68	231.03	0	0
TP-S-1511-33	direct	55.05	a		7		0.15	0.3	1	17468.24	846.39	0	0
TP-S-1511-34	direct	55.19	a		12		0.15	0.3	1	4009.22	211.41	0	0
TGL	direct	55.8	a		11		0.15	0.3	1	1014.18	89.61	0	0
LWQ	direct	53.44	a		11		0.15	0.3	1	1734.68	71.11	0	0
24K	direct	53.46	a		11		0.15	0.3	1	876.75	113.52	0	0
NMC	direct	53.55	a		11		0.15	0.3	1	600.68	45.91	0	0
MYL	direct	53.01	a		11		0.15	0.3	1	319.89	23.92	0	0
TP-S-1511-1	direct	48.83	a		3		0.15	0.3	1	1283.33	125.53	0	0
TP-S-1511-2	direct	49.05	a		6.8		0.15	0.3	1	468.71	54.14	0	0
TP-S-1511-3	direct	49.06	a		9		0.15	0.3	1	5093.10	352.58	0	0
TP-S-1511-4	direct	49.17	a		5		0.15	0.3	1	4192.93	213.11	0	0
TP-S-1511-5	direct	49.06	a		17.1		0.15	0.3	1	1084.93	109.12	0	0
TP-S-1511-6	direct	47.83	a		6.8		0.15	0.3	1	250.69	42.80	0	0
TP-S-1511-16	direct	48.6	a		9		0.15	0.3	1	886.69	86.78	0	0
TP-S-1511-27	direct	50.69	a		17		0.15	0.3	1	3586.99	323.06	0	0
TP-S-1511-28	direct	50.68	a		12		0.15	0.3	1	952.23	55.50	0	0
TP-S-1511-29	direct	50.66	a		24		0.15	0.3	1	255.93	26.86	0	0
TP-S-1511-30	direct	50.82	a		11		0.15	0.3	1	1343.22	127.57	0	0
TP-S-1511-31	direct	50.49	a		12		0.15	0.3	1	2117.49	238.03	0	0
TP-S-1511-32	direct	50.55	a		20		0.15	0.3	1	201.70	21.58	0	0
TP-S-1511-9	direct	47.95	a		12.5		0.15	0.3	1	3417.06	344.93	0	0
TP-S-1511-17	direct	48.56	a		15		0.15	0.3	1	822.01	92.20	0	0
TP-S-1511-18	direct	48.51	a		8		0.15	0.3	1	1277.70	101.71	0	0
TP-S-1511-21	direct	48.5	a		9		0.15	0.3	1	1079.43	101.39	0	0
TP-S-1511-22	direct	48.35	a		5		0.15	0.3	1	2201.12	226.49	0	0
TP-S-1511-23	direct	48.7	a		9		0.15	0.3	1	1072.04	104.53	0	0
TP-S-1511-24	direct	48.81	a		14		0.15	0.3	1	1042.25	109.11	0	0
TP-S-1511-25	direct	48.95	a		11.5		0.15	0.3	1	931.68	35.29	0	0
TP-S-1511-26	direct	48.98	a		12		0.15	0.3	1	759.41	65.26	0	0
TP-S-1511-8	direct	46.28	a		5		0.15	0.3	1	574.95	22.39	0	0

Table S3. Short-wave radiation input data at selected sites across the Tibetan Plateau close to the snow sampling sites.

		SW (W m^{-2})		SW (W m^{-2})
SETP				
	March, 2014	248	March, 2015	237
	April, 2014	288	April, 2015	259
	May, 2014	305	May, 2015	280
	June, 2014	265	June, 2015	250
NMC				
			March, 2015	264
			April, 2015	276
			May, 2015	306
			June, 2015	314
TGL				
	March, 2014	210		
	April, 2014	226		
	May, 2014	245		
	June, 2014	271		
LHG				
	March, 2014	229	March, 2015	238
	April, 2014	269	April, 2015	294
	May, 2014	311	May, 2015	305
	June, 2014	258	June, 2015	269

Supplementary Figures

Figure S1. Example of snow sampling sites over the Tibetan Plateau.

Figure S2. Snow grain size observation in the field (a) and measurement in the lab (b).

Figure S3. BC emissions arrived at the selected sites over the Tibetan Plateau based on data drawn from http://inventory.pku.edu.cn/download/download.html (Wang et al., 2014). (A value 2 on the x axis means 2×10^6 g month^{-1}. The BC value is averaged over 48 h along the back trajectory path. And the value on the y axis is the number of trajectories in the respective BC bin. The bin width is 0.05, i.e. from 0 to 5 on the horizontal axis there are 100 bins.)

Figure S3. Automatic weather stations selected for the short-wave radiation input data across the Tibetan Plateau.

Figure S4. BC emissions arrived at the selected sites over the Tibetan Plateau region based on data drawn from http://inventory.pku.edu.cn/download/download.html (Wang et al., 2014). (A value 2 on the x axis means 2×10^6 g month^{-1}. The BC value is averaged over 48 h along the back trajectory path. And the value on the y axis is the number of trajectories in the respective BC bin. The bin width is 0.05, i.e. from 0 to 5 on the horizontal axis there are 100 bins.)

Figure S5. Distributions of changes of snow cover duration days caused by BC and mineral dust.

Fig S1.

Figure S1. Example of snow sampling sites over the Tibetan Plateau.

Fig S2.

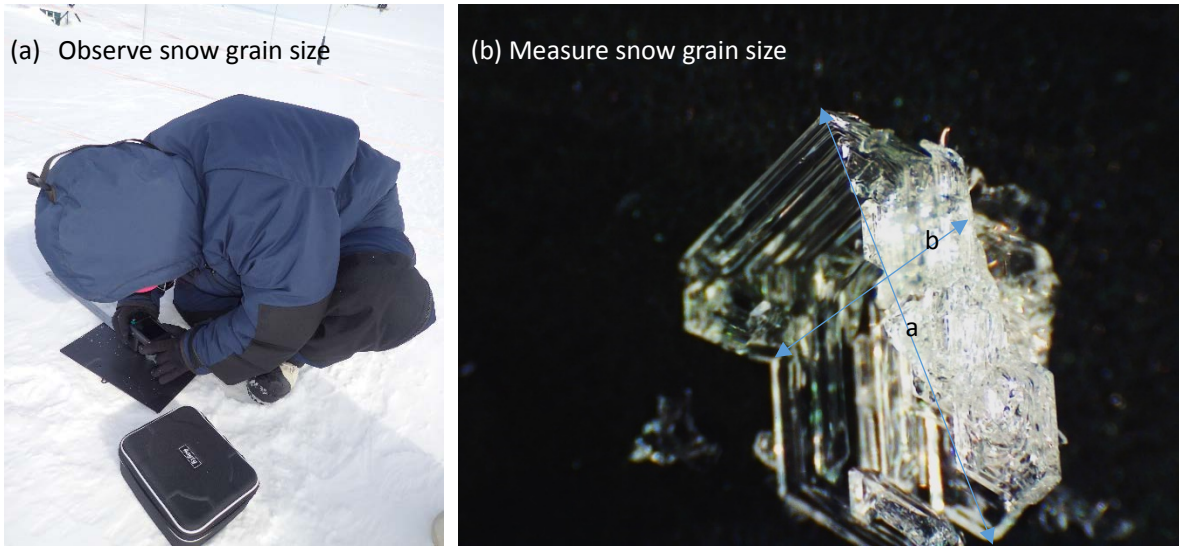

Figure S2. Snow grain size observation in the field (a) and measurement in the lab (b).

Fig S3.

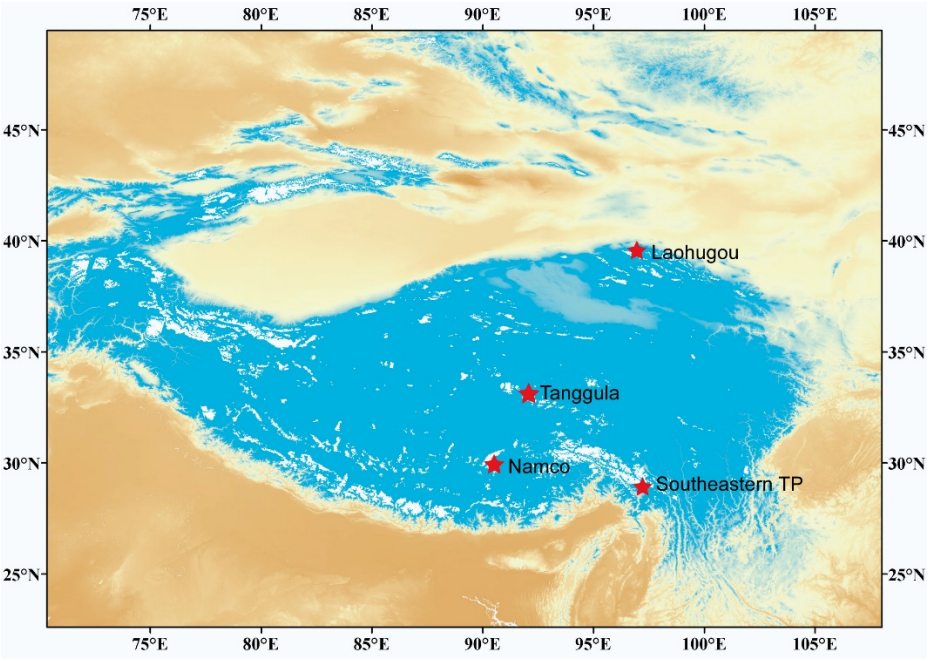

Figure S3. Automatic weather stations selected in the Tibetan Plateau.

Fig S4.

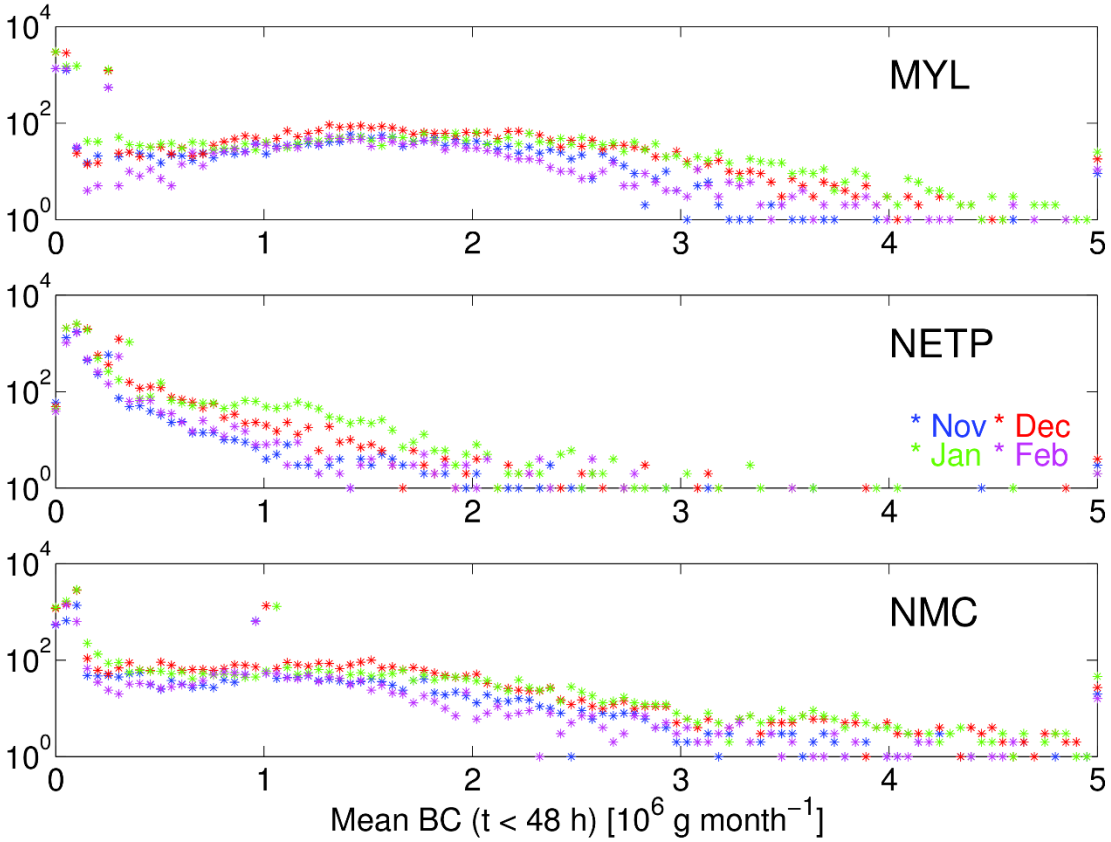

Figure S4. BC emissions arrived at the selected sites over the Tibetan Plateau region based on data drawn from http://inventory.pku.edu.cn/download/download.html (Wang et al., 2014). (A value 2 on the x axis means 2×10^6 g month^{-1}. The BC value is averaged over 48 h along the back trajectory path. And the value on the y axis is the number of trajectories in the respective BC bin. The bin width is 0.05, i.e. from 0 to 5 on the horizontal axis there are 100 bins.)

Fig S5.

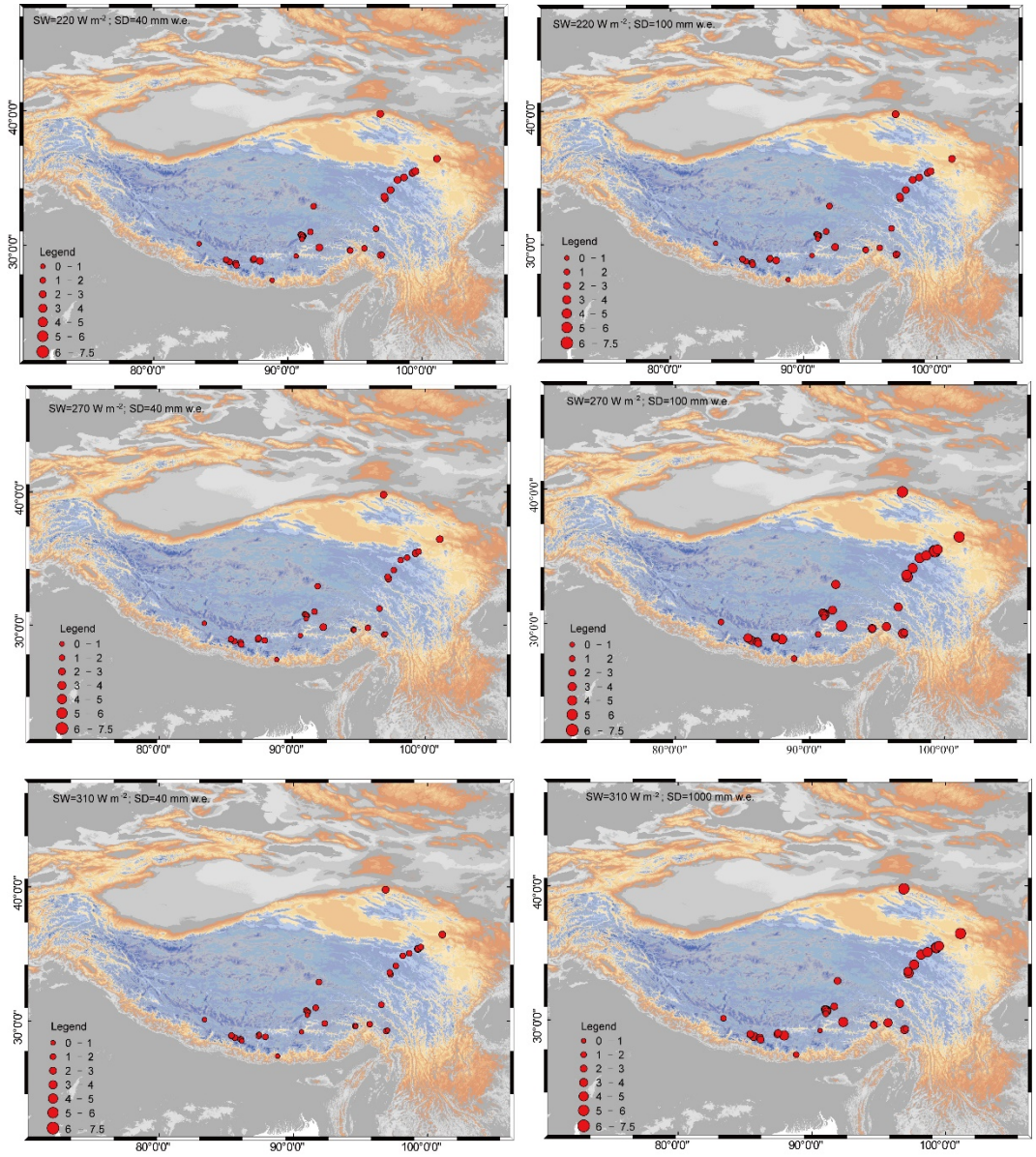

Figure S5. Distributions of changes of snow cover duration days caused by BC and mineral dust.

References:

Wang, R., Tao, S., Shen, H., Huang, Y., Chen, H., Baljanski, Y., Boucher, O., Ciais, P., Shen, G., Li, W., Zhang, Y., Chen, Y., Lin, N., Su, S., Li, B., Liu, J., Liu, W.: Trend in black carbon emissions from 1960 to 2007, Environ. Sci. Technol., doi:10.1021/es5021422, 2014.